BREAKTHROUGH REPORT

Chloroplast Acetyltransferase NSI Is Required for State Transitions in *Arabidopsis thaliana*

Minna M. Koskela[a,1], Annika Brünje[b,1], Aiste Ivanauskaite[a], Magda Grabsztunowicz[a], Ines Lassowskat[b,c], Ulla Neumann[d], Trinh V. Dinh[e, 2], Julia Sindlinger[f], Dirk Schwarzer[f], Markus Wirtz[e], Esa Tyystjärvi[a], Iris Finkemeier[b,c,*] and Paula Mulo[a,*]

[a]Department of Biochemistry, Molecular Plant Biology, University of Turku, Biocity A, Tykistökatu 6, 20520 Turku, Finland.
[b]Plant Physiology, Institute of Plant Biology and Biotechnology, University of Muenster, Schlossplatz 7, 48149 Münster, Germany.
[c]Plant Proteomics, Max Planck Institute for Plant Breeding Research, Carl-von-Linné-Weg 10, 50829 Cologne, Germany.
[d]Central Microscopy, Max Planck Institute for Plant Breeding Research, Carl-von-Linné-Weg 10, 50829 Cologne, Germany.
[e]Department of Plant Molecular Biology, Centre for Organismal Studies, Heidelberg University, 69120 Heidelberg, Germany.
[f]Interfaculty Institute of Biochemistry, University of Tübingen, Hoppe-Seyler-Str. 4, 72076, Tübingen, Germany.
[1]These authors contributed equally to this work.
[2]Present address: Institute of Biotechnology and Food Technology, Industrial University of Ho Chi Minh City, Ho Chi Minh City, Vietnam
[*]Shared corresponding authorship: Paula Mulo: pmulo@utu.fi; Iris Finkemeier: iris.finkemeier@uni-muenster.de

Running title: State transitions require NSI enzyme

One sentence summary: NSI is an active chloroplast Lys acetyltransferase required for state transitions in Arabidopsis independently of LHCII phosphorylation.

The authors responsible for distribution of materials integral to the findings presented in this article in accordance with the policy described in the Instructions for Authors (www.plantcell.org) are: Paula Mulo (pmulo@utu.fi) and Iris Finkemeier (iris.finkemeier@uni-muenster.de).

ABSTRACT

The amount of light energy received by the photosynthetic reaction centers photosystem II (PSII) and photosystem I (PSI) is balanced through state transitions. Reversible phosphorylation of a light harvesting antenna trimer (L-LHCII) orchestrates the association between L-LHCII and the photosystems thus adjusting the amount of excitation energy received by the reaction centers. In the present study, we identified the enzyme NUCLEAR SHUTTLE INTERACTING (NSI; AT1G32070) as an active lysine acetyltransferase in the chloroplasts of Arabidopsis (*Arabidopsis thaliana*). Intriguingly, *nsi* knock-out mutant plants

©2018 American Society of Plant Biologists. All Rights Reserved

were defective in state transitions, even though they had a similar LHCII phosphorylation pattern as wild type. Accordingly, *nsi* plants were not able to accumulate the PSI-LHCII state transition complex, even though the LHCII docking site of PSI and the overall amounts of photosynthetic protein complexes remained unchanged. Instead, the *nsi* mutants showed a decreased Lys acetylation status of specific photosynthetic proteins including PSI, PSII and LHCII subunits. Our work demonstrates that the chloroplast acetyltransferase NSI is needed for the dynamic reorganization of thylakoid protein complexes during photosynthetic state transitions.

INTRODUCTION

Light quality and quantity regulate photosynthetic light harvesting through dynamic reorganization of thylakoid membranes and the embedded protein complexes. A pool of LHCII trimers (L-LHCII) can function as an antenna either for photosystem (PS) II or PSI (Galka et al., 2012) and thereby adjust the amount of excitation energy received by the two photosystems (Allen, 1992). Changes in the association of L-LCHII between the reaction centers are referred to as state transitions, and they are regulated in a light-dependent manner via the reversible phosphorylation of L-LHCII subunits LHCB1 and LHCB2 (Bonaventura and Myers, 1969; Murata, 1969; Pietrzykowska et al., 2014). Upon illumination that leads to plastoquinone (PQ) pool reduction, LHCB1 and LHCB2 are phosphorylated by the STN7 kinase (Depège et al., 2003; Bellafiore et al., 2005), which results in increased absorbance of PSI (state 2). By contrast, illumination favoring PQ oxidation leads to dephosphorylation of LHCII by the PPH1/TAP38 phosphatase (Pribil et al., 2010; Shapiguzov et al., 2010) and energy distribution towards PSII (state 1). Specifically, phosphorylation of LHCB2 is required for the attachment of L-trimers to PSI via the PSAH subunit (Lunde et al., 2000; Crepin and Caffarri, 2015; Longoni et al., 2015), which results in the formation of a PSI-LHCII complex in the non-stacked regions of the thylakoid membrane (Kouřil et al., 2005). Additionally, some L-trimers appear to interact with PSI via the LHCA proteins (Benson et al., 2015). In C3 plants, state transitions have an important role in protecting PSI from photodamage under fluctuating light intensity (Grieco et al., 2012).

While phosphorylation is the best-studied post-translational modification regulating protein function, recent progress in enrichment techniques and high precision mass spectrometry have provided evidence that other modification types, such as the

reversible acetylation of lysine (Lys) residues, are abundant on chloroplast proteins as well (Finkemeier et al., 2011; Wu et al., 2011; Hartl et al., 2017; Schmidt et al., 2017). Lys acetylation was originally identified as a regulator of gene expression in the nucleus, where histone proteins undergo extensive acetylation/deacetylation by histone acetyltransferases and deacetylases. However, the acetylation machinery and the functional significance of Lys acetylation in chloroplasts have remained largely unknown. To gain insight into the role of Lys acetylation in the regulation of chloroplast function, we studied the Arabidopsis (*Arabidopsis thaliana*) enzyme NSI (NUCLEAR SHUTTLE INTERACTING; ATNSI; SNAT; AT1G32070). Based on its amino acid sequence NSI is predicted to contain an acetyltransferase domain and a chloroplast targeting transit peptide, which makes it a putative chloroplast acetyltransferase enzyme.

In the present study, we have employed quantitative mass spectrometry and *in vitro* Lys acetyltransferase assays to investigate the role of NSI as a lysine (Lys) acetyltransferase in Arabidopsis. The results showed that NSI is an active chloroplast-localized Lys acetyltransferase that affects the acetylation status of several chloroplast proteins. Since some of the affected proteins were found to be involved in the light reactions of photosynthesis, we further characterized the photosynthetic properties of two Arabidopsis knock-out lines lacking *NSI* (*nsi-1* and *nsi-2*). We found that the *nsi* mutants were not able to undergo state transitions in response to changes in illumination, even though the plants had wild-type (WT) levels of LHCII phosphorylation and the LHCII docking site on PSI was not impaired. In the light of our results, we propose that NSI is critical for the dynamic rearrangements of thylakoid membranes (i.e. state transitions). Possible mechanistic explanations will be discussed, but the exact mechanism for NSI action will remain an interesting topic for future research.

RESULTS

NSI is a chloroplast-localized Lys acetyltransferase

NSI localization was studied with a transient overexpression of NSI-YFP fusion protein in Arabidopsis protoplasts. The fusion protein clearly co-localized with chlorophyll autofluorescence, while no signal was detected in other compartments such as the nucleus (Figure 1). Immunoblotting of chloroplast fractions isolated from transgenic Arabidopsis lines expressing NSI-YFP further revealed that the majority of NSI is present in the soluble chloroplast fraction (Figure 1B). This observed plastid localization corroborates earlier results by Lee et al. (2014). To test whether NSI is able to function as a Lys acetyltransferase, an N-terminally His6-tagged recombinant protein lacking the predicted transit peptide (57 amino acids) was produced, and the Lys acetylation activity of the purified recombinant protein was examined on a general Lys acetyltransferase peptide substrate. NSI was indeed able to acetylate the ε-amino group of Lys residues using acetyl coenzyme A as a substrate (Figure 1C-D), indicating that NSI is an active chloroplast Lys acetyltransferase.

To examine the role of NSI in Lys acetylation of chloroplast proteins *in vivo*, we characterized two *nsi* knock-out mutant lines: *nsi-1* and *nsi-2* (Figure 2). Even though the visual phenotype of the *nsi* plants resembled that of the WT (Figure 2B) and they accumulated an equal amount of chlorophyll, the chlorophyll *a*/*b* ratio of the mutants was slightly lower compared to WT (Table 1). Additionally, our quantitative mass spectrometry (MS) analysis of the Lys acetylomes showed a decreased Lys acetylation level of several plastid proteins in both mutants as compared to WT (Figure 2C; Supplemental Dataset 1). Some of these proteins, including PSBP-1 (AT1G06680), PSAH-1/2 (AT3G16140; AT1G52230) and LHCB1.4 (AT2G34430) (Figure 2; Supplemental Dataset 1) are involved in the light reactions of photosynthesis. In particular, Lys acetylation on K88 of PSBP-1 was more than 12-fold down-regulated in both *nsi* mutants (LIMMA P-value ≤ 0.00018). Interestingly, some thylakoid proteins, such as LHCB6 (AT1G15820) and the ATPase β-subunit (ATCG00480), had slightly increased Lys acetylation levels in the mutants, suggesting

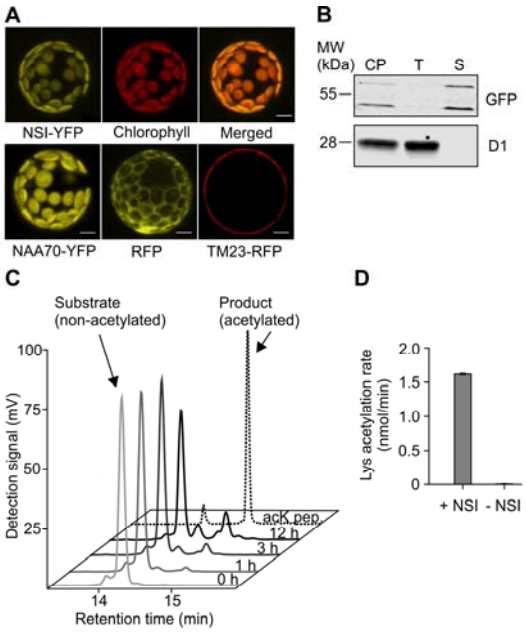

Figure 1. Localization and Lys acetylation activity of NSI. **A** Confocal microscopy image of Arabidopsis protoplast transiently expressing NSI-YFP (*35S:NSI-YFP*) fusion protein. Upper left panel shows the YFP signal, middle panel chlorophyll fluorescence of the same protoplast, and right panel is a merged image of the two. The lower panel shows the control lines: NAA70-YFP (left) was used as a chloroplast control marker, RFP (middle) as a cytoplasmic control and TM23-RFP (right) as a plasma membrane control. Scale bar is 10 µm. **B** Immunoblot detection of chloroplast protein fractions isolated from transgenic plants expressing NSI-YFP (*35S:NSI-YFP*) and separated on 12% acryl amide gel. GFP antibody was used for the detection of NSI-YFP and D1 antibody as a thylakoid membrane marker. NSI-YFP was detected as two bands, which may represent the preprotein (MW based on mobility = 61.0 kDa; expected MW = 56.5 kDa) and processed mature protein (MW based on mobility = 49.0 kDa; expected MW = 49.9 kDa). 10 µg of protein was loaded per sample (CP = chloroplasts, T = thylakoid fraction, S = soluble fraction). **C** HPLC analysis of a general lysine acetyltransferase substrate and its acetylated product after conversion by His6-NSI for 1, 3 or 12 h. Identities of non-acetylated (0 h) and acetylated (acK pep.) standard peptides were confirmed by MS. **D** Lysine acetylation rate of a peptide substrate by 10 µM His6-NSI (n = 3 technical replicates, ± SD).

that Lys acetylation in chloroplasts also occurs independently of NSI and that there is an interplay between the acetylation of different proteins. The decreased Lys acetylation status of the identified chloroplast proteins was not caused by changes in protein abundance, as the quantities of these proteins were similar between *nsi* and WT plants (Figure 2D; Supplemental Dataset 2). In addition, it has to be pointed out that NSI might control additional acetylation sites that cannot be detected with the trypsin-based digestion method, since peptide fragments might be generated that are either too big or too small for detection.

nsi knock-out plants have a defect in state transitions and are not able to form the PSI-LHCII complex in response to illumination

The decreased Lys acetylation status of PSII, PSI and LHCII prompted us to study the photosynthetic properties and organization of thylakoid protein complexes in the *nsi* mutants. In line with the unaffected growth phenotype of the *nsi* mutants, the

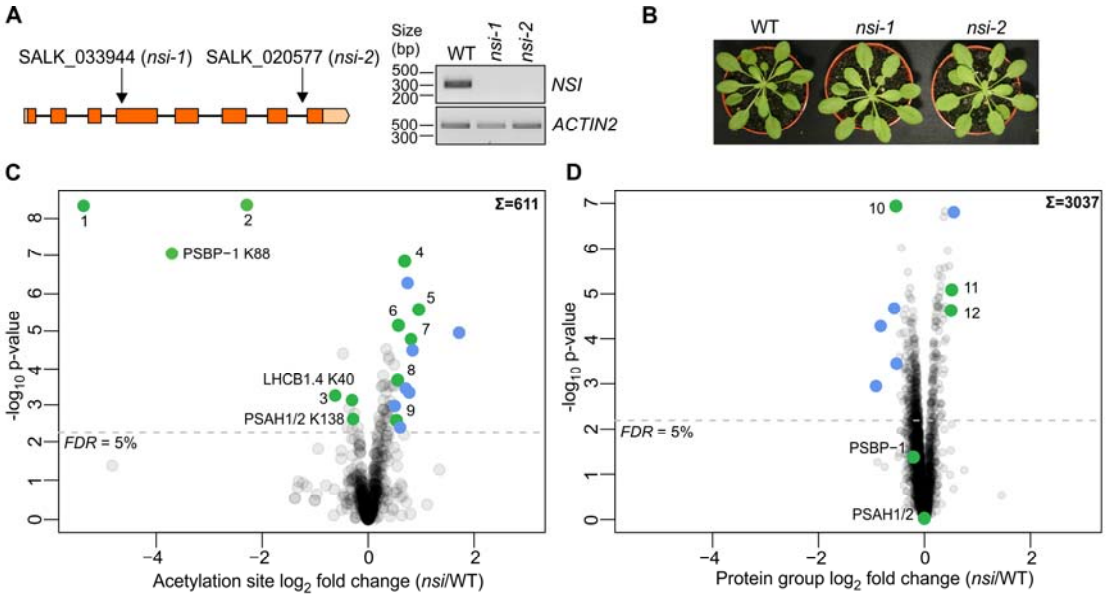

Figure 2. Characterization of the *nsi* knock-out lines and quantitative Lys acetylome analysis. **A** The left panel represents the gene model of *NSI* based on TAIR10. Positions of T-DNA insertions in each line are marked with arrows. Sand colored boxes represent 5'- and 3'-UTR regions, orange boxes exons and black lines introns.The right panel shows the absence of *NSI* mRNA verified with end-point RT-PCR. *ACTIN2* was used as a control of cDNA quality. **B** Phenotypes of 5-week-old WT and *nsi* mutant lines grown in short day (8 h light/ 16 h dark), PPFD 100 µmol m^{-2} s^{-1}, 50% humidity and +23°C. **C and D** Volcano plots representing quantitative Lys acetylome (**C**) and proteome (**D**) analyses of the *nsi* knock-out lines (*nsi-1* and *nsi-2*) compared to WT. Sums indicate numbers of quantified Lys acetylation sites and proteins, respectively. For statistical analyses, *nsi-1* and *nsi-2* were treated as group (defect in *NSI*) and tested against WT. Values had to be present in at least six out of the eight biological replicates. All replicate values are listed in the Supplemental Datasets 1 and 2. Green (plastid localization) and blue (non-plastid localization) circles illustrate significant data points with log_2-fold changes ≥ 0.5 or ≤ -0.5 and FDR corrected p-value ≤ 0.05 (LIMMA). Proteins involved in state transitions have been marked with text in the figure. 1: KEA1/2 K168/K170 (AT1G01790.1/AT4G00630.2), 2: unknown protein K62 (AT2G05310.1), 3: FER1 K134 (AT5G01600.1), 4: LHCB6 K220 (AT1G15820.1), 5: Plastid-lipid associated protein PAP K225 (AT3G26070.1), 6: ATPF K119 (ATCG00130.1), 7: SOUL heme-binding family protein K320 (AT5G20140.1), 8: SBPase K307 (AT3G55800.1), 9: ENH1 K233 (AT5G17170.1), 10: PSBH (ATCG00710.1), 11: ARM repeat superfamily protein (AT5G48120.1), 12: FAD6 (AT4G30950.1).

maximum quantum yield of PSII, represented as F_V/F_M, was similar to that of WT (Table 1). However, when we measured rapid light response curves of both chlorophyll fluorescence and P_{700} absorbance, a severe decrease in the yield of PSII was detected under low light intensities (Supplemental Dataset 3). This decrease was not due to an increase in NPQ, since the mutants showed similar or even slightly lower NPQ in low light intensities. However, the mutants seemed to have more closed PSII reaction centers, as shown by the decreased values of the coefficients of photochemical quenching (qP and qL) under these conditions (Supplemental Dataset 3), which can be a sign of excess excitation of PSII in these conditions. Intriguingly, in

152 higher light intensities this phenotype was lost or even reversed (Supplemental
153 Dataset 3).

154 To study the status of the photosynthetic electron transfer machinery further, we
155 extracted thylakoids from growth light (GL)-acclimated plants, solubilized the protein
156 complexes with different detergents and separated them with large pore blue native
157 gel electrophoresis (lpBN-PAGE). When thylakoids were solubilized with β-
158 dodecylmaltoside (DM; a detergent which solubilizes protein complexes from the
159 whole thylakoid membrane but breaks down labile interactions), no differences in the
160 abundances of any of the protein complexes between *nsi* and WT could be detected
161 (Figure 3). However, analysis of the *nsi* thylakoids solubilized with digitonin (a
162 detergent that preferentially solubilizes the PSI-rich stroma thylakoids and preserves
163 supramolecular interactions of the thylakoid protein complexes) revealed that the *nsi*
164 mutants lacked the PSI-LHCII complex in GL (Figure 3B) (Kouřil et al., 2005; Pesaresi
165 et al., 2009; Suorsa et al., 2015). This complex is composed of PSI, LHCI and LHCII
166 subunits (Supplemental Dataset 4; Pesaresi et al., 2009; Suorsa et al., 2015), and
167 accumulates in low to moderate light and upon transitioning from state 1 to state 2
168 (Kouřil et al., 2005; Pesaresi et al., 2009; Suorsa et al., 2015). In accordance with
169 previous findings (Suorsa et al., 2015), the complex was disassembled in the dark
170 (Figure 3B). Intriguingly, the megacomplex pattern of *nsi* closely resembled that of
171 *stn7* (Figure 3B) (Suorsa et al., 2015), which is the LHCII kinase mutant incapable of
172 performing state transitions (Depège et al., 2003; Bellafiore et al., 2005).

173 Moreover, an LC-MS/MS analysis was performed on the PSI-LHCII complex and the
174 LHCII trimers separated by the lpBN-PAGE to search for acetylation sites within the
175 complexes. However, for this analysis no immunoaffinity enrichment step for lysine-
176 acetylated peptides could be included due to the low amount of peptides retrieved
177 from the gel bands. First of all, the quantitative proteome analysis of the LHCII trimer
178 bands showed that the overall protein complex compositions was not different
179 between WT, *stn7* and both *nsi* mutants (Supplemental Dataset 4 A, C). Since the
180 PSI-LHCII complex was not present in the *nsi* mutants and in *stn7* (Figure 3B), this
181 complex was analyzed only in WT. Within this complex a few lysine-acetylated

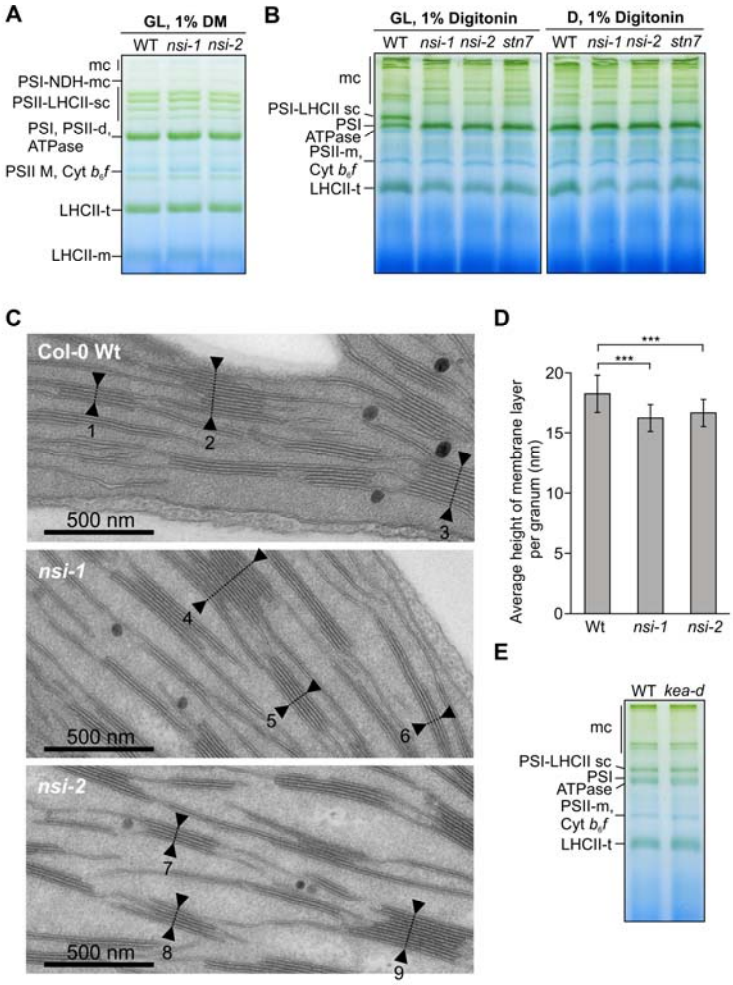

Figure 3. Organization of thylakoid protein complexes of WT, *nsi* and *stn7* and thylakoid ultrastructure of WT and *nsi*. **A** Large pore blue native gel of thylakoid protein complexes from thylakoids that were isolated from growth light (GL, 100 µmol photons m^{-2} s^{-1}) adapted plants and solubilized with 1% β-dodecylmaltoside (DM). Representative image from experiment repeated with three biological replicates is shown. (mc = megacomplex, sc = supercomplex, t = trimer, d = dimer, m = monomer). **B** Large pore blue native gels after digitonin solubilization of thylakoids isolated from plants after growth light (GL) or dark (D) adaptation. **C** Transmission electron microscopy (TEM) analysis of the *nsi* chloroplasts. TEM pictures of palisade mesophyll cells with chloroplasts in close-up view. Leaves of the two T-DNA insertion lines *nsi-1* and *nsi-2* and of wild-type Col-0 were prepared as thin section samples. Numbers and a rrows display exemplary thylakoid stacks. **D** Average heights per granum membrane layer ±SD for the two *nsi* knock-out lines in comparison to the wild type Col-0 (calculated from 3C). 700 thylakoid stacks per plant line displayed in 70 TEM pictures from seven independent biological replicates were analyzed (*** indicates p≤ 0.001 using two-tailed Student's t-test). **E** Large pore blue native gel of GL adapted WT and *kea1 kea2* double knock-out (*kea-d*) thylakoids solubilized with 1% digitonin.

proteins were identified, including PSAH (K99), LHCB1.2 (K44) and LHCB1.5 (K41) (Supplemental Dataset 4B). A few acetylation sites were also detected in the LHC trimers. Interestingly acetylation on the LHCB2.2 protein (Lys42, Lys120) was not detected in *nsi-1* and only detected in one replicate of *nsi-2*, while it was detected in 2-3 replicates of both *stn7* and WT (Supplemental Dataset 4D). Unfortunately, the lysine acetylation sites of PSAH1/2 (K138) and LHCB1.4 (K40), which were identified in the full acetylome analysis (Figure 2C), were not detected in this analysis, most

189 likely due to the missing immunoaffinity enrichment step. Furthermore, the thylakoid
190 preparation were done under native conditions, which makes it difficult to maintain the
191 *in vivo* acetylation status of all proteins.

192 Because of the observed changes in thylakoid protein organization, we also studied
193 the structure of *nsi* chloroplasts with transmission electron microscopy. In line with the
194 fact that *nsi* plants have no severe visual phenotype, they showed no major
195 differences in plastid ultrastructure compared to the WT (Figure 3C). However, the
196 grana stacks of the knock-out plants showed more compact packing than the WT
197 (Figure 3D).

198 Due to the absence of the PSI-LHCII state transition complex in *nsi*, we examined the
199 effect of NSI knock-out on state transitions further. First, we measured 77 K
200 fluorescence emission spectra of WT and *nsi* thylakoids. Thylakoids were extracted in
201 the middle of the light period (GL, 100 µmol photons m^{-2} s^{-1}) as well as at the end of
202 the dark period (D). In GL samples the fluorescence emission peak originating from
203 PSI (735 nm) was clearly lower in the *nsi* mutants than in WT, whereas the emission
204 spectra from D was similar between all lines (Figure 4). These results suggest that the
205 *nsi* mutant lines are defective in light-dependent adjustment of the excitation energy
206 distribution between PSII and PSI, i.e. state transitions. To confirm this conclusion, we
207 further investigated the behavior of *nsi* plants by treating them for 1 h in red (R; 660
208 nm; excites preferentially PSII) or far red (FR; 735 nm; excites preferentially PSI) light
209 to induce state 2 and state 1, respectively, and included the *stn7* mutant line as a
210 control. Thereafter, thylakoids were isolated and 77 K fluorescence emission spectra
211 were measured. Red light treatment induced state 2 in WT plants, while no such
212 effect could be detected in *nsi* or *stn7* (Figure 4B). Moreover, *in vivo* fluorescence
213 measurements with a pulse amplitude modulation fluorometer confirmed that state
214 transitions in all mutant lines were very weak and significantly different from the WT
215 (Figure 4C, Table 1).

216 KEA1 and/or KEA2 were among the most drastically downregulated Ac-Lys targets
217 detected in *nsi* (Figure 2C). KEA1 and KEA2 are chloroplast envelope K^+/H^+

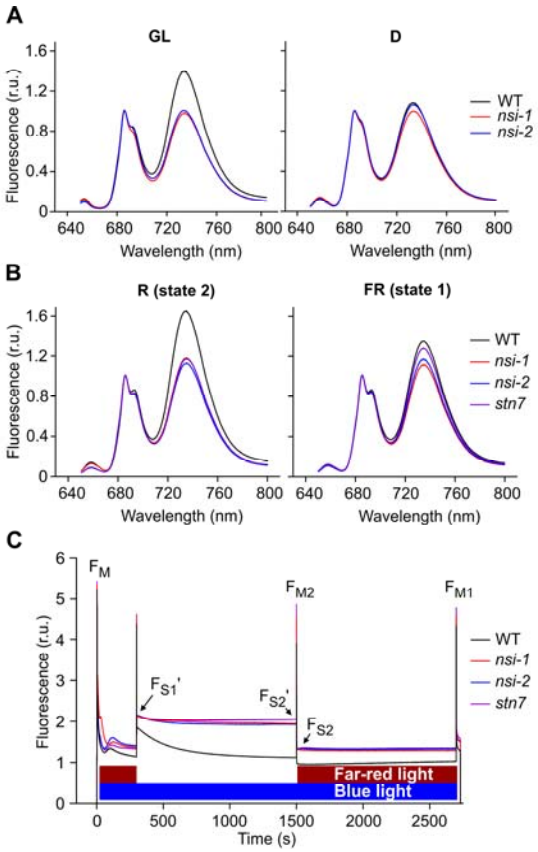

Figure 4. State transitions in WT, *nsi* and *stn7* under different light treatments. **A** 77 K fluorescence emission spectra from thylakoids isolated from growth light (GL)- and dark (D)-adapted plants. **B** 77 K fluorescence emission spectra from thylakoids isolated from red (R; 660 nm)- or far red light (FR; 735 nm)-treated plants. Spectra in A-B have been normalized to 685 nm and present an average of three biological replicates. Fluorescence emission around 685-695 nm originates from PSII and fluorescence emission around 735 nm from PSI. **C** Representative graphs of state transition measurements with a pulse amplitude modulation fluorometer.

antiporters, which are essential for chloroplast pH and osmoregulation (Kunz et al. 2014). Because *kea1 kea2* double knock-out mutants showed impaired partitioning of the proton motive force across the thylakoid membrane, the function of the KEA transporters appears to be linked to the photosynthetic light reactions (Kunz et al. 2014). Therefore, we studied state transitions in the *kea1 kea2* plants. However, no defects were detected in state transitions (qT = 0.10 ± 0.01, n = 12) or in the accumulation of the PSI-LHCII complex in the *kea1 kea2* plants (Figure 3E), suggesting that inactivation of the KEA transporters does not result in impaired state transitions.

LHCII phosphorylation and the PSI docking site for LHCII are not impaired in *nsi*

228 Since phosphorylation of LHCII, and especially that of the LHCB2 subunit of the L-
229 LHCII trimers, has been shown to be the main determinant of state transitions (Leoni
230 et al., 2013; Pietrzykowska et al., 2014; Crepin and Caffarri, 2015; Longoni et al.,
231 2015), we analyzed the phosphorylation status of thylakoid proteins of *nsi* mutants by
232 immunoblotting with a phospho-threonine (P-Thr) antibody. No differences were
233 detected between the *nsi* mutants and WT in the overall phosphorylation status of
234 thylakoid proteins isolated from growth light or darkness (Figure 5). In addition, after
235 red (state 2) light treatment LHCII was found to be phosphorylated in *nsi* and WT
236 plants whereas, as expected, no phosphorylation was seen in *stn7* (Figure 5B). Far
237 red light treatment led to LHCII dephosphorylation in all lines (Figure 5B). To analyze
238 LHCII phosphorylation in more detail, we immunoblotted thylakoids isolated from GL-
239 adapted plants with (phospho) LHCB1 and LHCB2 antibodies. Figure 5C shows that
240 phosphorylation levels of both of these proteins, but especially that of LHCB2, were
241 even higher in *nsi* than in the WT, even if the total amounts appeared similar or
242 slightly lower in the signal from the immunoblot. However, no differences in LHCB1
243 and LHCB2 abundances between WT and mutants were detected by quantitative
244 mass spectrometry (Supplemental Dataset 2), which suggests that there was less
245 efficient binding of antibody to the hyperphosphorylated LHCB1/2. Because L-LHCII
246 has been shown to interact with PSI through the PSAH subunit (Crepin and Caffarri,
247 2015; Longoni et al., 2015; Lunde et al., 2000) or through the LHCA antenna (Benson
248 et al., 2015), we also checked *nsi* for the abundance of these proteins. Both proteins
249 were present similar in abundance in the mutants compared to WT (Figure 5D).
250 Taken together, we conclude that the inability of *nsi* plants to undergo state transitions
251 is not due to impaired LHCII phosphorylation or defects in the PSI docking sites for L-
252 LCHII.

253

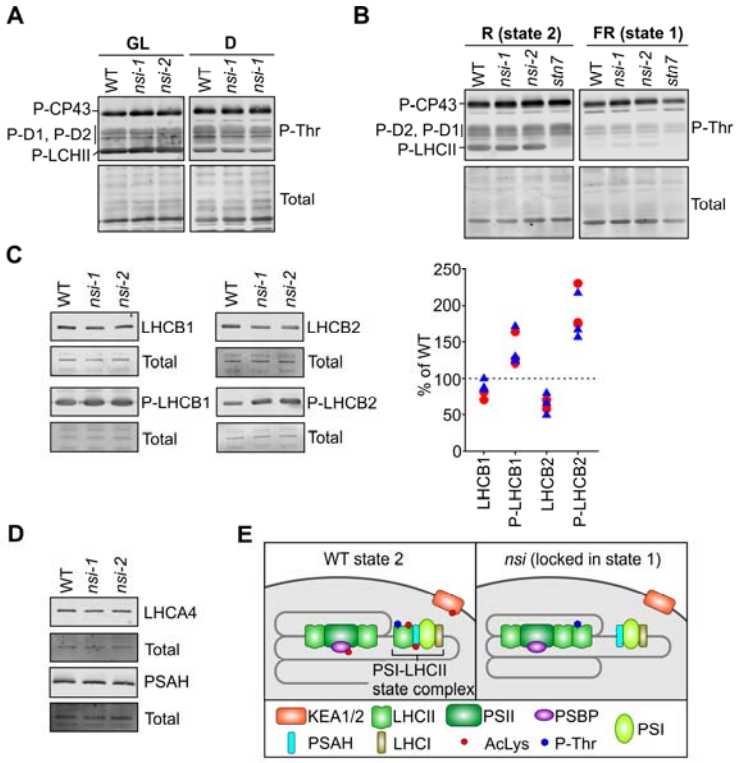

Figure 5. Immunoblot analysis of thylakoid protein phosphorylation, L-LHCII subunits and PSI docking site for L-LHCII and schematic presentation of the downregulated Lys acetylation sites in *nsi*. **A** Phosphorylation of thylakoid proteins isolated from growth light (GL)- or dark (D)-adapted plants. Proteins were separated on 15% acryl amide gels and immunoblotted with P-Thr antibody. **B** Phosphorylation of thylakoid proteins isolated form R- or FR-treated plants. Proteins were separated on 12% acryl amide gels and immunoblotted with P-Thr antibody. **C** Analysis of L-LHCII subunits from GL-adapted thylakoids. Proteins were separated on 12% acrylamide gels and immunoblotted using antibodies against LHCB1 and LHCB2 and their phosphoforms (P). Right panel shows quantification of LHCB1, LHCB2 and their phosphorylated forms in *nsi* mutants (*nsi-1* is marked with red circles and *nsi-2* with blue triangles). Protein amounts were quantified from the blots and calculated as a percentage of WT from the respective replicate. **D** Immunoblot analysis of L-LHCII docking site on PSI. Proteins were isolated from GL-adapted plants, separated on 12% acrylamide gels and immunoblotted with PSAH and LHCA4 antibodies. The lower panels (Total) show blots after staining with REVERT™ total protein stain to verify equal loading; representative blots are shown from three biological replicates (A-D). **E** Comparison of chloroplast protein complexes between WT and *nsi* in state 2. Upon conditions favoring plastoquinone pool reduction, L-LHCII trimers are phosphorylated, which results in the interaction of L-LHCII with PSI, mediated by PSAH (state 2 in WT). In contrast to WT, P-LHCII is not able to interact with PSI in *nsi* under state 2 conditions. The phenotype may result from defects in Lys acetylation of (i) PSAH and LHCII, which may hinder the PSI-LHCII interaction, or (ii) PSBP and LHCII, which may result in a strong interaction between PSII and L-LHCII, or (iii) proteins involved in chloroplast ion homeostasis (PSBP, KEA1/KEA2), which may be required for the dynamic reorganization of thylakoid protein complexes.

DISCUSSION

Despite the fact that Lys acetylation of various chloroplast proteins and the first plastid Lys deacetylase have been recently identified (Finkemeier et al., 2011; Wu et al., 2011; Hartl et al., 2017; Schmidt et al., 2017), the chloroplast Lys acetyltransferase enzymes have not been characterized to date. Nevertheless, Lys acetylation has been shown to have marked effects on chloroplast function, as it regulates the activities of Rubisco, Rubisco activase, and phosphoglycerate kinase enzymes (Finkemeier et al., 2011; Hartl et al., 2017) as well as the stability of ATP synthase

262 (Schmidt et al., 2017). Here we have identified a plant organellar Lys
263 acetyltransferase, NSI, which is localized in the chloroplast stroma (Figure 1). Loss of
264 NSI affected the acetylation status of various chloroplast proteins, including PSAH-
265 1/PSAH-2, LHCB1.4, PSBP-1 and KEA1/ KEA2 (Figure 2C, Supplemental Dataset 1).
266 In addition, *nsi* plants were not able to carry out light-dependent reorganization of
267 thylakoid protein complexes (i.e. state transitions) (Figure 3 and 4). Intriguingly, the
268 *nsi* mutants closely resembled *stn7*, even though LHCII phosphorylation in *nsi* was
269 not impaired (Figure 5). This finding suggests that NSI affects state transitions
270 independently of LHCII phosphorylation.

271 In WT plants, state transitions occur as a response to plastoquinone pool reduction or
272 oxidation (state 2 and state 1, respectively). Under state 2 conditions, the STN7
273 kinase is activated and phosphorylates the L-LHCII trimer composed of LHCB1 and
274 LHCB2 subunits. The phosphorylated trimer then binds to PSI via the PSAH subunit
275 (together with the nearby PSAO and PSAL subunits), increasing the absorption cross
276 section of PSI (Lunde et al., 2000; Zhang and Scheller 2004; Galka et al., 2012).
277 Recently, also the LHCA proteins, localized on the opposite site of PSI as compared
278 to PSAH, have been implicated in binding a pool of L-LHCII trimers (Benson et al.,
279 2015). Lack of acetylation in one or more of these proteins might disturb direct
280 protein-protein interactions, which are required for light energy transfer from LHCII to
281 PSI. Indeed, we observed a small but consistent 1.2-fold decrease in Lys acetylation
282 of PSAH-1/2 in *nsi* mutants. Additionally, a similar decrease in the acetylation status
283 of LHCB1.4, an abundant subunit in the L-LHCII trimers (Galka et al. 2012), was
284 detected in the *nsi* plants (Figure 2C). Since acetylation, in general, can affect the
285 conformation of a protein and furthermore removes the charge of the Lys residue,
286 adequate acetylation of one or more of these proteins may be necessary for a stable
287 interaction between the thylakoid protein complexes (Figure 5E). It is noteworthy that
288 the LHCII-PSI state transition complex has been shown to be composed of one L-
289 LHCII attached to one PSI reaction center via the PSAH subunit (Kouřil et al., 2005)
290 and that this complex was completely absent in *nsi* (Figure 3B). Indeed, the state
291 transition phenotype in the *PSAH* co-suppression line was similar to *nsi* (Lunde et al.,

292 2000). It should be noted, however, that the effect of NSI to state transitions might
293 also be mediated via the formation of the PSII supercomplexes: changes in the
294 acetylation of PSII and LHCII subunits might result in permanent attachment of L-
295 LHCII to PSII, which could prevent L-LHCII binding to PSI (Figure 5E).

296 As LHCII phosphorylation and an intact L-LHCII docking site of PSI have been shown
297 to be indispensable for state transitions (Lunde et al., 2000; Depège et al., 2003;
298 Zhang and Scheller 2004; Bellafiore et al., 2005; Galka et al., 2012), practically all
299 mutants defective in state transitions have problems either in the accumulation or
300 phosphorylation of LHCII, or in the LHCII docking site of PSI. For instance, other
301 mutations affecting the accumulation of LHCII, e.g. *chlorina1-2* with impaired
302 chlorophyll *b* biosynthesis and *chaos* deficient in cpSRP43, have an effect on state
303 transitions, either due to the decreased level of LHCII phosphorylation in *chlorina1-2*
304 or the lack of L-LHCII in *chaos* (Wang and Grimm 2016). The PSB33 protein, which
305 provides stability to PSII-LHCII supercomplexes, is also indispensable for proper
306 phosphorylation of the thylakoid proteins upon fluctuating light conditions, and
307 therefore affects accumulation of PSI-LHCII complexes and state transitions (Fristedt
308 et al. 2015, 2017). The *ics1* mutants with dysfunctional ISOCHORISMATE
309 SYNTHASE 1 (ICS1) protein, involved in the biosynthesis of phylloquinone and
310 salicylic acid, possess higher PQ pool reduction levels and increase numbers of
311 stacked thylakoids per granum as compared to WT (Gawronski et al. 2013).
312 Moreover, the decreased content of phylloquinone results in defective in state
313 transitions in *ics1* (Gawronski et al. 2013). However, as the level of LHCII
314 phosphorylation in this mutant was not studied, speculation on the mechanistic details
315 behind the defective state transitions is not possible (Gawronski et al. 2013).

316 The complex interactions between the chloroplasts and mitochondria in
317 *Chlamydomonas reinhardtii* have been exemplified by examining the photosynthetic
318 properties of mutants having defects in mitochondrial respiratory electron transfer
319 (Cardol et al. 2003, Schönfeld et al. 2004). The respiration rates of the *dum* mutants
320 were shown to correlate with the relative quantum yield of photosynthetic electron
321 transfer, and the mutants were not able to perform transition to state 1, apparently

322 because of an increased rate of non-photochemical PQ pool reduction and persistent
323 LHCII phosphorylation even under illumination with PSI light (Cardol et al. 2003). By
324 contrast, the *Chlamydomonas reinhardtii stm6* mutants showing reduced levels of
325 cytochrome *c* oxidase and rotenone-insensitive external NADPH dehydrogenase
326 activities, were locked in state 1 (Schönfeld et al. 2004). The LHCII phosphorylation in
327 *stm6* was impaired even if the PQ pool was in a more reduced state as compared to
328 WT, possibly because of over-reduction of stroma resulting in inactivation of the STN7
329 kinase (Schönfeld et al. 2004; Rintamäki et al. 2000). These examples show that even
330 if state transitions in *Chlamydomonas reinhardtii* tune the ratio between linear and
331 cyclic photosynthetic electron transfer, thus responding to the metabolic need for ATP
332 (Wollman 2001) rather than balancing energy distribution between the two
333 photosystems (as in plants), the mechanistic background of state transitions is always
334 based on reversible LHCII phosphorylation. LHCII phosphorylation, however, may be
335 differently regulated, and indeed no such tight interplay between respiration and state
336 transitions has been reported in higher plants as compared to *Chlamydomonas*
337 *reinhardtii*.

338 Thylakoid membrane architecture shows large rearrangements during state
339 transitions, and unstacking of grana occurs upon transition to state 2 (Chuartzman et
340 al. 2008). Interestingly, the grana in the *nsi* were more tightly packed than in the WT
341 (Fig. 3C). On the other hand, as chloroplast ion content is known to be a key
342 determinant of thylakoid membrane stacking, it can play an important role in state
343 transitions in conjunction with LHCII phosphorylation (Kaňa and Govindjee, 2016).
344 Indeed, one of the most drastically down-regulated Lys acetylation sites in the *nsi*
345 mutants was found in the PSBP-1 protein, where acetylation was more than 12-fold
346 less abundant than in WT (Figure 2C). The PSBP-1 protein is a lumenal PSII subunit
347 that stabilizes Ca^{2+} and Cl^{-} binding in the oxygen evolving complex (OEC) (Ifuku et al.,
348 2008). Intriguingly, the altered Lys acetylation site of PSBP-1 is situated in the N-
349 terminal domain (K88 of the preprotein; K11 in the mature protein), which is essential
350 for ion binding and oxygen evolution (Ifuku et al., 2005; 2008). It has previously been
351 shown that defects in the function of PSBP-1 affect thylakoid structure (Yi et al., 2009)

352 and that a correct composition of the oxygen evolving complex influences state
353 transition kinetics (Allahverdiyeva et al., 2013). Therefore, it is possible that lack of
354 acetylation might alter ion binding by PSBP-1 in *nsi*, which could disrupt the protein
355 complex reorganization required for state transitions.

356 Another strongly affected site was found in a peptide that is common to the KEA1 and
357 KEA2 proteins. KEA1 and KEA2 are homologous K^+/H^+ antiporters localized in the
358 chloroplast envelope (Kunz et al., 2014). Double knock-out *kea1 kea2* plants are
359 severely affected in their growth and contain malformed, swollen chloroplasts, which
360 underlines the importance of a proper ion balance in chloroplasts (Kunz et al., 2014).
361 It is thus possible that the lack of acetylation in KEA1 and KEA2 proteins (Figure 2C)
362 could cause the compact thylakoid stacking detected in *nsi* chloroplasts (Figure 3C-D)
363 through altered ion content in the chloroplast, which in turn might lead to obstruction
364 of protein complex reorganization (Figure 5E). If this is the case, acetylation is most
365 likely required for the inactivation of KEA channels in WT, since state transitions in the
366 *kea1 kea2* mutant plants were fully functional. Whether acetylation of KEA1 and KEA2
367 is involved in channel inactivation, and thereby has an influence on ion homeostasis
368 and state transitions, remains to be tested.

369 Our present results reveal a new layer in the dynamic regulation of chloroplast light
370 responses and implicate the chloroplast acetyltransferase NSI as a prerequisite for
371 state transitions (Figure 5E). In addition to *nsi* and the docking site mutant *psah*, no
372 other mutants have yet been described that have a WT-like growth phenotype, no
373 defects in LHCII phosphorylation, but lack state transitions. This is an intriguing
374 finding that correlates with the function of NSI as a Lys acetyltransferase, and with a
375 decreased acetylation status of a number of chloroplast proteins. Although the causal
376 relationship between the LHCII phosphorylation and state transitions was described
377 long ago (Bennett et al. 1980; Allen, 1992), numerous questions around the ways in
378 which Lys acetylation could play a role have remained unanswered. For instance,
379 what kind of effect(s) does the three-dimensional structure of the thylakoid network
380 have on the state transitions, and how are changes in chloroplast ion content reflected
381 in state transitions *in vivo*? Are components other than LHCB1, LHCB2, PSAH and

382 PSI subunits in the vicinity of PSAH required for state transitions? Are there still other,
383 so-far uncharacterized factors regulating state transitions? Whether the effect of NSI
384 on state transitions is based directly on Lys acetylation and disturbed interaction
385 between PSI and LHCII, on altered PSII-LHCII interaction or on some other more
386 indirect mechanism that affects thylakoid dynamics, will be important topics for further
387 investigation.

388 **MATERIALS AND METHODS**

389 **Plant material**

390 *Arabidopsis thaliana* (Col-0) was grown in 8 h light/16 h darkness at photosynthetic
391 photon flux density (PPFD) of 100 µmol m^{-2} s^{-1} (light source: Osram powerstar HQI-BT
392 400W/D daylight), 50% humidity and +23°C. Seed stocks for the *nsi* (At1g32070) T-
393 DNA lines and WT were ordered from the Nottingham Arabidopsis stock center
394 (NASC), and *stn7* (SALK_073254) was received from Dr. Mikko Tikkanen (Tikkanen
395 et al., 2006). The two *nsi* T-DNA lines SALK_033944 and SALK_020577 (*nsi-1* and
396 *nsi-2*, respectively) were PCR screened according to Salk Institute Genomic Analysis
397 Laboratory instructions and using primers *nsi-1*: LP: 5'-
398 AAGAAGTCCCCAGTAACAATCC and RP: 5'-CCGCCTTCTGTGTCAAATAAC; *nsi-2*:
399 LP: 5'-CGAGCTGATTTACGTGGAAAG and RP: 5'-AGCTTATTGGTATGGCACGTG;
400 BP for both lines was LBb1.3 (5'-ATTTTGCCGATTTCGGAAC). Absence of *NSI*
401 mRNA was verified with end-point RT-PCR using gene-specific primers and *ACTIN2*
402 as a control (NSI_fw_1: 5'-GATTCATCAGAAGGCGGGGAT, NSI_rev_1: 5'-
403 GATGCCTTCTGGATCAGCCT, ACTIN2_fw: 5'-GTGAACGATTCCTGGACCTGCCTC
404 and ACTIN2_rev: 5'-GAGAGGTTACATGTTCACCACAAC). RNA was extracted using
405 Agilent Plant RNA Isolation Mini Kit and treated with Ambion TURBO DNA-free™
406 DNAse. cDNA was synthesized with Bio-Rad iScript™ cDNA Synthesis Kit.

407 **Determination of chlorophyll content**

408 Leaf discs were cut, weighed and incubated overnight in 1 ml of dimethylformamide
409 (DMF) in darkness and RT. Chlorophyll content was calculated according to (Inskeep
410 and Bloom, 1985).

411 **Generation of transgenic YFP-line**

412 A transgenic Arabidopsis line expressing NSI with a C-terminal YFP-tag (*35S:NSI-*
413 *YFP*) was generated via modified floral inoculation (Narusaka et al., 2010) using
414 *Agrobacterium tumefaciens* GV3101:pMP90:pSoup. The coding sequence of NSI was
415 amplified from Arabidopsis cDNA using NSI_fw_2: 5'-
416 TATACCCGGGATGCTACTAATCCCA and NSI_rev_2: 5'-
417 TATAGGATCCCTTTGGGTACCAAAACATG. The PCR product was cloned into
418 pGWR8-YFP (Rozhon et al., 2010), which was used for the transformation.

419 **Fluorescence microscopy**

420 Detection of YFP-fusion proteins was performed as previously described (Dinh et al.,
421 2015). Signal of the red fluorescence protein (RFP) was recoded using a 560-615 nm
422 band-filter after excitation at 543 nm. Primers for expression of full-length NSI protein
423 as an N-terminal fusion of YFP were: NSI_fw_3: 5'-
424 GATCGGATCCATGCTACTAATCCCAATTTC and NSI_rev_3: 5'-
425 GATCGTCGACCTTTGGGTACCAAAACATGC. Localization of marker proteins in the
426 chloroplast (NAA70-YFP), the cytosol (RFP) and the plasma-membrane (TMD23-
427 RFP) have been demonstrated earlier in (Dinh et al., 2015) and (Brandizzi et al.,
428 2002), respectively.

429 **Thylakoid protein extraction**

430 Fresh Arabidopsis leaves were ground 3 × 2 s in cold buffer (300 mM sucrose, 50 mM
431 HEPES-KOH pH 7.6, 5 mM $MgCl_2$, 1 mM Na-EDTA, 1.25% BSA, 22 mM ascorbate,
432 10 mM NaF). Homogenate was filtered through Miracloth (Millipore) and the filtrate
433 was centrifuged for 4 min, 4000 *g*, +4°C to pellet chloroplasts and thylakoids.
434 Chloroplasts were broken by resuspending the pellet to hypotonic lysis buffer (5 mM
435 sucrose, 10 mM Hepes-KOH pH 7.6, 5 mM $MgCl_2$, 10 mM NaF, Pierce™ protease
436 inhibitor (Thermo Scientific)). The lysate was centrifuged at 18 000 *g* for 5 min, +4°C,
437 and the pellet (thylakoids) was resuspended in storage buffer (100 mM sucrose, 10
438 mM Hepes-KoH pH 7.6, 10 mM $MgCl_2$, 10 mM NaF). Different biological replicates

439 were prepared from plants grown at different times on separate trays. The chlorophyll
440 concentration of thylakoids was determined as described (Porra et al., 1989).

441 **Chloroplast isolation and fractionation**

442 Fresh Arabidopsis rosettes were ground 3 × 2 s in cold buffer (330 mM sorbitol, 50
443 mM HEPES-KOH pH 7.6, 1 mM $MgCl_2$, 5 mM Na-EDTA, 0.1% BSA, 5 mM
444 ascorbate). Leaf homogenate was filtered through one layer of Miracloth (Millipore)
445 and the filtrate centrifuged for 2 min, 2000 *g*, +4°C. The pellet was gently
446 resuspended into residual buffer. Chloroplast suspension was loaded on top of a
447 Percoll step gradient (40%/80% Percoll in 330 mM sorbitol, 50 mM HEPES-KOH pH
448 7.6) and centrifuged 6 min, 7000 *g,* +4°C with mild acceleration and no breaks in a
449 fixed angle rotor. Intact chloroplasts were collected from the gradient interface, and
450 washed twice (330 mM sorbitol, 50 mM HEPES-KOH pH 7.6, 2 mM Na-EDTA).
451 Chloroplasts were pelleted 2 min, 10 000 *g*, +4°C and resuspended into hypotonic
452 lysis buffer (5 mM sucrose, 10 mM Hepes-KOH pH 7.6, 5 mM $MgCl_2$) at a final
453 concentration of 1 µg chlorophyll/µl buffer. Suspension was freeze-thawed with liquid
454 nitrogen and fractions separated by centrifuging 10 min, 18 000 *g*, +4°C. Supernatant
455 was collected as the soluble fraction. The pellet (thylakoids) was washed and finally
456 resuspended into storage buffer (100 mM sucrose, 10 mM Hepes-KoH pH 7.6, 10 mM
457 $MgCl_2$). Protein concentrations were determined with Bradford Protein Assay (Bio-
458 Rad).

459 **Immunoblotting of thylakoids and chloroplast fractions**

460 Proteins were solubilized with 2 × Laemmli buffer (Laemmli, 1970) supplemented with
461 6 M urea and run on 12 or 15% acrylamide gels, as indicated, containing 6 M urea.
462 The gels were blotted to Immobilon®-FL (Merck Millipore) membrane in blotting buffer
463 (39 mM glycine, 48 mM Tris, 1.3 mM SDS, 20% MeOH) using 1 mA/cm^2 for 1 h with
464 Hoefer TE77X semi-dry blotter. All blots were blocked using 5% BSA in TTBS (20 mM
465 Tris-HCl pH 7.5, 150 mM NaCl, 0.05% Tween 20). Rabbit P-Thr antibody was
466 purchased from New England Biolabs (NEB) and used as a 1:3000 dilution with 0.5
467 µg of chlorophyll. Rabbit LHCA4 (AS01 008), LHCB1 (AS01 004), LHCB2 (AS01

468 003), P-LHCB1 (AS13 2704, lot 1310), P-LHCB2 (AS13 2705, lot 1310) and PSAH
469 (AS06 105) antibodies were purchased from Agrisera and used as 1:5000 (LHCB1,
470 LHCB2, PSAH) or 1:10 000 (P-LHCB1 and P-LHCB2) dilutions (Leoni et al., 2013).
471 Rabbit GFP antibody (SAB4301138, lot 492635538) was purchased from Sigma and
472 used as a 1:5000 dilution. Rabbit D1 DE-loop antibody (Kettunen et al., 1996) was
473 used as a 1:8000 dilution. LI-COR Goat anti-rabbit IRDye® 800CW 2nd antibody was
474 used for detection according to manufacturer's instructions. Blots were imaged using
475 LI-COR Odyssey CLx. Blots were stained with REVERT™ Total Protein Stain (LI-
476 COR) to verify equal loading and transfer of proteins.

477 **Native electrophoresis**

478 Large-pore blue native gels and samples were prepared as previously described
479 (Järvi et al., 2011).

480 **Heterologous expression and purification of recombinant NSI protein**

481 *NSI* coding sequence, excluding that for the predicted transit peptide (57 N-terminal
482 amino acid residues), was amplified from Arabidopsis cDNA with Phusion High
483 Fidelity Polymerase (Thermo Scientific). The sequence was amplified using
484 NSI_fw_4: 5'-CAAGGATCCTCTGGGTTTGTGAAG and NSI_rev_4: 5'-
485 GTACCCGGGCTACTTTGGGTACCA primers. The *NSI* PCR product was cloned into
486 pQE-30 vector (Qiagen). Protein was expressed in BL21(DE3)pLysS cells (Invitrogen)
487 induced with 1 mM IPTG (Roth) for 15 hours at 21 °C. Cells were harvested,
488 resuspended in buffer (100 mM Tris-HCl pH 7.8, 150 mM NaCl, protease inhibitor
489 cocktail (Sigma)) and disrupted with a French press. After addition of 5 mM DTT and
490 10 U lysozyme recombinant NSI was purified from the soluble phase by Protino® Ni-
491 NTA affinity chromatography (Macherey-Nagel). Proteins were eluted with 500 mM
492 imidazole and desalted on PD-10 gel filtration columns (GE Healthcare) using 50 mM
493 Tris-HCl (pH 7.8), 150 mM NaCl, 10% glycerol. The protein concentrations were
494 determined with Pierce 660 nm Protein Assay (Thermo Scientific).

495 **Lys acetyltransferase activity assay**

496 The acetyltransferase activity assay was performed by incubating His6-NSI (10 µM)
497 and a general Lys acetyltransferase peptide substrate (50 µM) coupled to anthranilic
498 acid at the N-terminus at 30°C in reaction buffer (150 mM Na-phosphate pH 7, 50 mM
499 NaCl) (Seidel et al., 2016). Reaction was started by addition of 50 µM Ac-CoA. 20 µl
500 samples were collected from time points between 0 and 12 h, and the reaction was
501 stopped by addition of 180 µL trifluoroacetic acid (TFA, final concentration 2%).
502 Reaction products were analyzed by reversed phase HPLC chromatograph
503 (Shimadzu Corp.) equipped with CBM-20A controller, 2 LC-20AD pumps, DGU-20A
504 degasser, SPD-20A detector and SIL-20AC autosampler. Separation was achieved
505 on a Hypersil GOLD column (4.6 mm x 250 mm, 5 µm particle size; Thermo
506 Scientific). A gradient program consisting of solvent A (0.1% TFA (v/v) in distilled
507 water) and solvent B (95% acetonitrile, 0.1% TFA (v/v) in distilled water) was applied
508 at a flow rate of 1.0 mL/min as follows: 0-1 min: 5% B, 1-20 min: linear 5-100% B, 20-
509 25 min: 100% B, 25-25.5 min: 100-5% B, 25.5-30 min: 5% B. 100 µL of sample
510 solution was injected. The detector was set at 218 (peptide backbone) and 360 nm
511 (anthranilic acid). All reaction rates were determined from three independent technical
512 replicates. Reaction rates were calculated from the peak areas of the free Lys and Ac-
513 Lys peptides, which eluted at 14.34 and 14.85 min, respectively.

514 **Protein extraction, peptide dimethyl labeling and Lys-acetylated peptide**
515 **enrichment**

516 Frozen leaf material was ground to fine powder in liquid nitrogen and extracted using
517 a modified filter-assisted sample preparation (FASP) protocol (Wiśniewski et al.,
518 2009a) and treated as described in (Wiśniewski et al., 2009b). Digested peptides
519 were dimethyl labeled on C18 Sep-Pak plus short columns (Waters) as previously
520 described (Boersema et al., 2009). Equal amounts of light and medium labeled
521 peptides were pooled for each replicate and the solvent evaporated in a vacuum-
522 centrifuge. 15 µg of peptide mixture was stored for whole proteome analysis. Lys-
523 acetylated peptide enrichment was performed as previously described (Hartl et al.,
524 2015) with 8 mg peptide per combined sample (1 mg peptide/25 µL antibody slurry).

525 After enrichment the eluted peptides were desalted and fractionated in three steps
526 using SDB Stagetips (Kulak et al., 2014) and evaporated in a vacuum centrifuge.

527 **LC-MS/MS data acquisition**

528 Dried peptides were dissolved in 2% ACN, 0.1% TFA for analysis. Samples were
529 analyzed using an EASY-nLC 1200 (Thermo Fisher) coupled to a Q Exactive HF
530 mass spectrometer (Thermo Fisher). Peptides were separated on 17 cm frit-less silica
531 emitters (New Objective, 0.75 µm inner diameter), packed in-house with reversed-
532 phase ReproSil-Pur C18 AQ 1.9 µm resin (Dr. Maisch). The column was kept at 50°C
533 in a column oven throughout the run. The following parameters were used for whole
534 proteome analysis, and parameters for acetylome analysis are stated in brackets; if
535 not stated separately parameters are identical. Peptides were eluted for 115 (68) min
536 using a segmented linear gradient of 0% to 98% solvent B (solvent A 0% ACN, 0.5%
537 FA; solvent B 80% ACN, 0.5% FA) at a flow-rate of 300 (250) nL/min. Mass spectra
538 were acquired in data-dependent acquisition mode with a Top15 method. MS spectra
539 were acquired in the Orbitrap analyzer with a mass range of 300–1759 m/z at a
540 resolution of 60 000 (120 000) FWHM, maximum IT of 55 ms and a target value of 3 ×
541 106 ions. Precursors were selected with an isolation window of 1.3 (1.2) m/z. HCD
542 fragmentation was performed at a normalized collision energy of 25. MS/MS spectra
543 were acquired with a target value of 105 (5 × 104) ions at a resolution of 15 000
544 FWHM, maximum IT of 55 (150) ms and a fixed first mass of m/z 100. Peptides with a
545 charge of +1, greater than 6, or with unassigned charge state were excluded from
546 fragmentation for MS2, and dynamic exclusion for 30 s prevented repeated selection
547 of precursors.

548 **MS data analysis**

549 Raw data were processed using MaxQuant software version 1.5.2.8
550 (http://www.maxquant.org/) (Cox and Mann, 2008; Tyanova et al., 2016a). MS/MS
551 spectra were searched with the Andromeda search engine against the TAIR10
552 database (TAIR10_pep_20101214;
553 ftp://ftp.arabidopsis.org/home/tair/Proteins/TAIR10_protein_lists/). Sequences of 248

554 common contaminant proteins and decoy sequences were automatically added during
555 the search. Trypsin specificity was required and a maximum of two (proteome) or four
556 missed cleavages (acetylome) were allowed. Minimal peptide length was set to seven
557 amino acids. Carbamidomethylation of cysteine residues was set as fixed, oxidation of
558 methionine and protein N-terminal acetylation as variable modifications. Acetylation of
559 lysines was set as variable modification only for the antibody enriched samples. Light
560 and medium dimethylation of lysines and peptide N-termini were set as labels.
561 Peptide-spectrum-matches and proteins were retained if they were below a false
562 discovery rate of 1%, modified peptides were additionally filtered for a score ≥ 35 and
563 a delta score of ≥ 6 to remove low quality identifications. Match between runs and
564 requantify options were enabled. Downstream data analysis was performed using
565 Perseus version 1.5.5.3 (Tyanova et al., 2016b). For proteome and acetylome,
566 reverse hits and contaminants were removed, the site ratios log_2 transformed, and
567 flip-label ratios inverted. Plotting of the raw and the normalized site ratios confirmed
568 that the automatic normalization procedure of MaxQuant worked reliably and
569 normalized site ratios were used for all further analyses. For quantitative Lys
570 acetylome analyses, sites were filtered for a localization probability of ≥ 0.75. The
571 "expand site table" feature of Perseus was used to allow separate analysis of site
572 ratios for multiply acetylated peptides occurring in different acetylation states.
573 Technical replicates were averaged and sites as well as protein groups displaying
574 less than two out of four ratios were removed. The resulting matrices for proteome
575 and acetylome, respectively, were exported and significantly differential abundant
576 protein groups and Lys acetylation sites were determined using the LIMMA package
577 (Ritchie et al., 2015) in R 3.3.1 (R core team, 2016). Volcano plots were generated
578 with R base graphics, plotting the non-adjusted P-values vs. the log_2 fold-change and
579 marking data points below 5% FDR (i.e. adjusted P-values) when present.

580 **Trypsin-digestion of bands excised from lpBN-PAGE and data analysis**

581 Protein spots were excised from gels, trypsin digested as described before (Morgan et
582 al., 2008), and analyzed using LC-MS/MS. Raw data were processed using
583 MaxQuant software version 1.5.2.8 (http://www.maxquant.org/) (Cox and Mann, 2008;

584 Tyanova et al., 2016a). MS/MS spectra were searched with the Andromeda search
585 engine against the Araport 11 database. Sequences of 248 common contaminant
586 proteins and decoy sequences were automatically added during the search. Trypsin
587 specificity was required and a maximum of two missed cleavages were allowed.
588 Minimal peptide length was set to seven amino acids. Carbamidomethylation of
589 cysteine residues was set as fixed, and oxidation of methionine as variable
590 modifications. Acetylation of lysines and phosphorylation (STY) were set as variable
591 modification. Peptide-spectrum-matches and proteins were retained if they were
592 below a false discovery rate of 1%, a score ≥ 35 and a delta score of ≥ 6 for modified
593 peptides were required. Match between runs and iBAQ were enabled. Downstream
594 data analysis was performed using Perseus version 1.6.1.3 (Tyanova et al., 2016b).
595 Reverse hits and contaminants were removed, and peptide and iBAQ intensities were
596 log2 transformed. Technical replicates were averaged and sites as well as protein
597 groups identified in only one replicate of each genotype were removed. Data were
598 analyzed from three independent biological replicates.

599 **Fluorescence measurements**

600 77 K fluorescence emission spectra were measured from thylakoids diluted with
601 storage buffer to 0.33 µg/ml chlorophyll. Each spectrum was measured with QEPro
602 spectrometer (Ocean Optics) from a 100 µl thylakoid batch using 3 s integration time
603 and blue excitation light.

604 Rapid light response curves were measured with Dual-PAM-100 (Heinz Walz GmbH)
605 equipped with DUAL-E emitter and DUAL-DR detector units, using a red measuring
606 beam for fluorescence and red actinic light. Absorbance changes due to oxidation of
607 the primary donor P_{700} of PSI were measured simultaneously with the same device at
608 830 nm. One leaf from an intact Arabidopsis rosette was used per biological replicate.
609 Measurements were done after 20 min of dark incubation followed by determination of
610 initial fluorescence F_0 with the measuring beam alone, F_M with a saturating flash, and
611 maximum P_{700} oxidation (P_M) (Klughammer and Schreiber, 1994) by a saturating flash
612 preceded by 10 s FR illumination. Thereafter, each measurement continued by 2 min

613 illumination steps, with a saturating flash at the end of each step to allow the
614 determination of parameters of PSII and PSI as follows. The quantum yield of PSII,
615 Y(II) (Genty et al., 1989), non-photochemical quenching, NPQ (Demmig-Adams,
616 1990), photochemical quenching, qP (Schreiber et al., 1986) and qL (Kramer et al.,
617 2004), the quantum yield of regulated and non-regulated non-photochemical
618 quenching, Y(NPQ) and Y(NO), respectively (Kramer et al., 2004) were calculated
619 from the fluorescence data and the quantum yield of PSI, Y(I) and the donor and
620 acceptor side limitation of PSI, Y(ND) and Y(NA), respectively (Klughammer and
621 Schreiber, 1994) were calculated from absorbance changes at 830 nm. One leaf from
622 an intact rosette was used per biological replicate.

623 State transitions were measured using a Waltz PAM-101 fluorometer equipped with
624 the FIP control software (Tyystjärvi and Karunen, 1990) using dark incubated (30 min)
625 plants. First, F_0 and F_M were measured from a dark acclimated leaf, and the values
626 were used to calculate F_V/F_M ($F_V = F_M – F_0$). Then, the leaf was illuminated for 5 min
627 with FR LED (Walz 102-FR, 53 µmol photons m^{-2} s^{-1}) and blue LED (470 nm LED
628 filtered through a 470 nm, 10 nm FWHM filter (Androver Corporation), 24 µmol m^{-2} s^{-1})
629 to activate photosynthesis. Then the FR was turned off for 20 min to induce state 2,
630 after which it was turned on again for 20 min to induce state 1. At the end of each
631 illumination step, a saturating pulse was fired to obtain maximum fluorescence in state
632 1 (F_{M1}') or state 2 (F_{M2}'). The state transition parameters qT and qS were calculated
633 according to (Ruban and Johnson, 2009). One detached leaf from one Arabidopsis
634 rosette was used per biological replicate. White-light saturating pulses (1 s, PPFD
635 2750 µmol m^{-2} s^{-1}) and the measuring beam of the PAM-101 fluorometer were used.

636 **Sample preparation for Transmission Electron Microscopy (TEM)**

637 Leaf discs (2 mm) from six-week-old WT and mutant plants cultivated in 8 h light/16 h
638 darkness were excised using a biopsy punch, fixed with 2.5% (v/v) glutaraldehyde
639 and 2% (w/v) paraformaldehyde in 0.05 M sodium cacodylate buffer (pH 6.9) for 3 h at
640 room temperature and then kept overnight at 4 °C. Subsequently, samples were
641 rinsed six times for 10 minutes in 0.05 M sodium cacodylate buffer (pH 6.9, rinse 3

642 and 4 supplemented with 0.05 M glycine) and postfixed in 1% osmium tetroxide in
643 0.05M sodium cacodylate (pH 6.9) supplemented with 0.15% potassium ferricyanide
644 for 1 h on ice. After thorough rinsing in 0.05 M sodium cacodylate buffer (pH 6.9) and
645 water, samples were further dehydrated with a series of ethanol, gradually transferred
646 to acetone and embedded into Araldite 502/Embed 812 resin (EMS, catalog number
647 13940) using the ultrarapid infiltration by centrifugation method revisited by
648 (McDonald, 2014). Ultrathin (70-90 nm) sections were collected on nickel slot grids as
649 described by (Moran and Rowley, 1987), stained with 0.1% potassium permanganate
650 in 0.1N H_2SO_4 (Sawaguchi et al., 2001) and examined with an Hitachi H-7650 TEM
651 (Hitachi High-Technologies Europe GmbH, Krefeld, Germany) operating at 100 kV
652 fitted with an AMT XR41-M digital camera (Advanced Microscopy Techniques,
653 Danvers, USA). Leaf samples of seven biological replicates per genotype were
654 analyzed. For each of those leaf samples, 10 images at a magnification of 10,000
655 were taken from chloroplast areas from palisade parenchyma with a section
656 orientation perpendicular to the majority of thylakoid membranes. In total, membrane
657 layers and grana heights from 700 grana stacks per genotype were quantified.

658 **Statistical analyses**

659 Experimental plant material was grown appropriately blocked for each experiment.
660 Statistical analysis of chlorophyll content and fluorescence measurements was
661 performed with IBM SPSS Statistics software. For the quantitative MS data,
662 differential protein and peptide abundances from four independent biological
663 replicates were tested with the LIMMA package (Ritchie et al., 2015) in R 3.3.1 (R
664 core team, 2016). For statistical analysis of the membrane layers per grana height
665 data was analyzed in Microsoft Excel using a two-tailed Student's t-test assuming
666 unequal variances.

667 **Accession Numbers**

668 The MS proteomics data have been deposited to the ProteomeXchange Consortium
669 via the PRIDE (Vizcaíno et al., 2016) partner repository with the dataset identifier
670 PXD007625 and PXD007630. *NSI* (At1g32070) T-DNA lines used in this work were

671 *nsi-1* (SALK_033944) and *nsi-2* (SALK_020577), and *STN7* (At1g68830) T-DNA line
672 *stn7* (SALK_073254).

673 **Supplemental data**

674 Supplemental Dataset 1: Quantitative acetylome data analysis.
675 Supplemental Dataset 2: Quantitative proteome data analysis.
676 Supplemental Dataset 3: Fast light response curves of P700 absorbance and
677 chlorophyll fluorescence.
678 Supplemental Dataset 4: Quantitative proteome data analysis of the PSI-LHCII, PSI,
679 and LHCII trimer bands excised from the lpBN-PAGE.
680 Supplemental File 1: ANOVA tables.

681 **Author contributions** P.M., I.F., M.M.K., E.T., D.S. and M.W. designed the
682 experiments, M.M.K., A.B., A.I., M.G., I.L., U.N., T.V.D. and J.S. performed research,
683 and M.M.K., P.M., I.F., I.L., A.B. and E.T. analyzed the data. M.M.K., P.M. and I.F.
684 wrote the manuscript and all authors revised and approved it.

685 **Acknowledgements**
686 Dr. Taina Tyystjärvi and Dr. Daniel Gibbs are thanked for reading the manuscript, and
687 Dr. Hans-Henning Kunz for providing the *kea* seeds. This study was financially
688 supported by Academy of Finland (307335 “Centre of Excellence in Molecular Biology
689 of Primary Producers” for P.M., M.M.K., A.I., M.G. and E.T. and 259075 for E.T.),
690 Doctoral Programme in Molecular Life Sciences at the University of Turku and The
691 Finnish Concordia Fund for M.M.K., the “Professorinnenprogramm” of the University
692 of Muenster for A.B. and I.F., the Max Planck Gesellschaft for I.L., U.N. and I.F., and
693 the Deutsche Forschungsgemeinschaft (FI 1655/3-1, INST 211/744-1 FUGG) for I.F.
694 Selected aspects of this work were supported by the German research foundation
695 funds SFB 1036/TP13 and WI 3560/2-1 for M.W. This project was carried out within
696 the ERA-CAPS Research Programme “KatNat”.

697

Table 1. Chlorophyll content and state transition parameters of WT, *nsi* and *stn7*. Differences between genotypes were tested with ANOVA (Supplemental File 1). All data were normally distributed, apart from the *stn7* qT parameter, and variances were homogenous. Multiple comparisons were done with Tukey HSD. Averages ± SD are shown, and n is marked in brackets.

Plant line	Chl *a*+*b* (µg/mg) [a)]	Chl *a*/*b* [b)]	F_V/F_M [c,f)]	qT [d,g)]	qS [e,h)]
WT	1.32 ± 0.11 (n=27)	3.50 ± 0.14	0.79 ± 0.04 (n=4)	0.10 ± 0.01	0.80 ± 0.02
nsi-1	1.34 ± 0.12 (n=27)	3.44 ± 0.13	0.81 ± 0.01 (n=4)	0.01 ± 0.01	0.23 ± 0.03
nsi-2	1.27 ± 0.11 (n=27)	3.40 ± 0.13	0.81 ± 0.02 (n=4)	0.01 ± 0.01	0.25 ± 0.03
stn7	1.26 ± 0.11 (n=14)	3.36 ± 0.10	0.82 ± 0.01 (n=4)	-0.01 ± 0.01	0.08 ± 0.04

a) ANOVA P = 0.079.
b) ANOVA P = 0.005; Multiple comparisons: WT vs. *nsi-1* P = 0.322, WT vs. *nsi-2* P = 0.025, WT vs. *stn7* P = 0.009, *nsi-1* vs. *nsi-2* P = 0.649, *nsi-1* vs. *stn7* P = 0.264, *nsi-2* vs. *stn7* P = 0.820.
c) ANOVA P = 0.294.
d) ANOVA P = 1.493×10^{-8}; Multiple comparisons: WT vs. *nsi-1* P = 1.168×10^{-7}, WT vs. *nsi-2* P = 1.852×10^{-7}, WT vs. *stn7* P = 2.151×10^{-8}, *nsi-1* vs. *nsi-2* P = 0.953, *nsi-1* vs. *stn7* P = 0.216, *nsi-2* vs. *stn7* P = 0.094.
e) ANOVA P = 1.385×10^{-12}; Multiple comparisons: WT vs. *nsi-1* P = 2.266×10^{-11}, WT vs. *nsi-2* P = 3.052×10^{-11}, WT vs. *stn7* P = 2.512×10^{-12}, *nsi-1* vs. *nsi-2* P = 0.894, *nsi-1* vs. *stn7* P = 0.007×10^{-2}, *nsi-2* vs. *stn7* P = 0.027×10^{-3}.
f) $F_V/F_M = (F_M-F_0)/F_M$
g) qT = $(F_{M1}-F_{M2})/F_{M1}$, where F_{M1} and F_{M2} are the maximum fluorescence yields after illumination causing state 1 and 2, respectively.
h) qS = $(F_{S1}'-F_{S2}')/(F_{S1}'-F_{S2})$, where $F_{S1'}$ and $F_{S2'}$ are fluorescence yields in the beginning and at the end, respectively, of illumination causing state 2, and F_{S2} is fluorescence yield immediately after switching on illumination causing state 1.

Figure legends

Figure 1. Localization and Lys acetylation activity of NSI. **A** Confocal microscopy image of Arabidopsis protoplast transiently expressing NSI-YFP (*35S:NSI-YFP*) fusion protein. Upper left panel shows the YFP signal, middle panel chlorophyll fluorescence of the same protoplast, and right panel is a merged image of the two. The lower panel shows the control lines: NAA70-YFP (left) was used as a chloroplast control marker, RFP (middle) as a cytoplasmic control and TM23-RFP (right) as a plasma membrane control. Scale bar is 10 µm. **B** Immunoblot detection of chloroplast protein fractions isolated from transgenic plants expressing NSI-YFP (*35S:NSI-YFP*) and separated on 12% acrylamide gel. GFP antibody was used for the detection of NSI-YFP and D1 antibody as a thylakoid membrane marker. NSI-YFP was detected as two bands, which may represent the preprotein (MW based on mobility = 61.0 kDa; expected MW = 56.5 kDa) and processed mature protein (MW based on mobility = 49.0 kDa; expected MW = 49.9 kDa). 10 µg of protein was loaded per sample (CP = chloroplasts, T = thylakoid fraction, S = soluble fraction). **C** HPLC analysis of a general lysine acetyltransferase substrate and its acetylated product after conversion by His6-NSI for 1, 3 or 12 h. Identities of non-acetylated (0 h) and acetylated (acK pep.) standard peptides were confirmed by MS. **D** Lysine acetylation rate of a peptide substrate by 10 µM His6-NSI (n = 3 technical replicates, ± SD).

Figure 2. Characterization of the *nsi* knock-out lines and quantitative Lys acetylome analysis. **A** The left panel represents the gene model of *NSI* based on TAIR10.

740 Positions of T-DNA insertions in each line are marked with arrows. Sand colored
741 boxes represent 5'- and 3'-UTR regions, orange boxes exons and black lines introns.
742 The right panel shows the absence of *NSI* mRNA verified with end-point RT-PCR.
743 *ACTIN2* was used as a control of cDNA quality. **B** Phenotypes of 5-week-old WT and
744 *nsi* mutant lines grown in short day (8 h light/ 16 h dark), PPFD 100 µmol m^{-2} s^{-1}, 50%
745 humidity and +23°C. **C and D** Volcano plots representing quantitative Lys acetylome
746 (**C**) and proteome (**D**) analyses of the *nsi* knock-out lines (*nsi-1* and *nsi-2*) compared
747 to WT. Sums indicate numbers of quantified Lys acetylation sites and proteins,
748 respectively. For statistical analyses, *nsi-1* and *nsi-2* were treated as group (defect in
749 *NSI*) and tested against WT. Values had to be present in at least six out of the eight
750 biological replicates. All replicate values are listed in the Supplemental Datasets 1 and
751 2. Green (plastid localization) and blue (non-plastid localization) circles illustrate
752 significant data points with log_2-fold changes ≥ 0.5 or ≤ -0.5 and FDR corrected p-
753 value ≤ 0.05 (LIMMA). Proteins involved in state transitions have been marked with
754 text in the figure. 1: KEA1/2 K168/K170 (AT1G01790.1/AT4G00630.2), 2: unknown
755 protein K62 (AT2G05310.1), 3: FER1 K134 (AT5G01600.1), 4: LHCB6 K220
756 (AT1G15820.1), 5: Plastid-lipid associated protein PAP K225 (AT3G26070.1), 6:
757 ATPF K119 (ATCG00130.1), 7: SOUL heme-binding family protein K320
758 (AT5G20140.1), 8: SBPase K307 (AT3G55800.1), 9: ENH1 K233 (AT5G17170.1), 10:
759 PSBH (ATCG00710.1), 11: ARM repeat superfamily protein (AT5G48120.1), 12:
760 FAD6 (AT4G30950.1).

761 **Figure 3.** Organization of thylakoid protein complexes of WT, *nsi* and *stn7* and
762 thylakoid ultrastructure of WT and *nsi*. **A** Large pore blue native gel of thylakoid
763 protein complexes from thylakoids that were isolated from growth light (GL, 100 µmol
764 photons m^{-2} s^{-1}) adapted plants and solubilized with 1% β-dodecylmaltoside (DM).
765 Representative image from experiment repeated with three biological replicates is
766 shown. (mc = megacomplex, sc = supercomplex, t = trimer, d = dimer, m = monomer).
767 **B** Large pore blue native gels after digitonin solubilization of thylakoids isolated from
768 plants after growth light (GL) or dark (D) adaptation. **C** Transmission electron
769 microscopy (TEM) analysis of the *nsi* chloroplasts. TEM pictures of palisade
770 mesophyll cells with chloroplasts in close-up view. Leaves of the two T-DNA insertion
771 lines *nsi-1* and *nsi-2* and of wild-type Col-0 were prepared as thin section samples.
772 Numbers and arrows display exemplary thylakoid stacks. **D** Average heights per
773 granum membrane layer ±SD for the two *nsi* knock-out lines in comparison to the wild
774 type Col-0 (calculated from 3C). 700 thylakoid stacks per plant line displayed in 70
775 TEM pictures from seven independent biological replicates were analyzed (***
776 indicates p≤ 0.001 using two-tailed Student's t-test). **E** Large pore blue native gel of
777 GL adapted WT and *kea1 kea2* double knock-out (*kea-d*) thylakoids solubilized with
778 1% digitonin.

779 **Figure 4.** State transitions in WT, *nsi* and *stn7* under different light treatments. **A** 77 K
780 fluorescence emission spectra from thylakoids isolated from growth light (GL)- and
781 dark (D)-adapted plants. **B** 77 K fluorescence emission spectra from thylakoids
782 isolated from red (R; 660 nm)- or far red light (FR; 735 nm)-treated plants. Spectra in
783 A-B have been normalized to 685 nm and present an average of three biological

784 replicates. Fluorescence emission around 685-695 nm originates from PSII and
785 fluorescence emission around 735 nm from PSI. **C** Representative graphs of state
786 transition measurements with a pulse amplitude modulation fluorometer.

787 **Figure 5.** Immunoblot analysis of thylakoid protein phosphorylation, L-LHCII subunits
788 and PSI docking site for L-LHCII and schematic presentation of the downregulated
789 Lys acetylation sites in *nsi*. **A** Phosphorylation of thylakoid proteins isolated from
790 growth light (GL)- or dark (D)-adapted plants. Proteins were separated on 15%
791 acrylamide gels and immunoblotted with P-Thr antibody. **B** Phosphorylation of
792 thylakoid proteins isolated form R- or FR-treated plants. Proteins were separated on
793 12% acrylamide gels and immunoblotted with P-Thr antibody. **C** Analysis of L-LHCII
794 subunits from GL-adapted thylakoids. Proteins were separated on 12% acrylamide
795 gels and immunoblotted using antibodies against LHCB1 and LHCB2 and their
796 phosphoforms (P). Right panel shows quantification of LHCB1, LHCB2 and their
797 phosphorylated forms in *nsi* mutants (*nsi-1* is marked with red circles and *nsi-2* with
798 blue triangles). Protein amounts were quantified from the blots and calculated as a
799 percentage of WT from the respective replicate. **D** Immunoblot analysis of L-LHCII
800 docking site on PSI. Proteins were isolated from GL-adapted plants, separated on
801 12% acrylamide gels and immunoblotted with PSAH and LHCA4 antibodies. The
802 lower panels (Total) show blots after staining with REVERT™ total protein stain to
803 verify equal loading; representative blots are shown from three biological replicates
804 (A-D). **E** Comparison of chloroplast protein complexes between WT and *nsi* in state 2.
805 Upon conditions favoring plastoquinone pool reduction, L-LHCII trimers are
806 phosphorylated, which results in the interaction of L-LHCII with PSI, mediated by
807 PSAH (state 2 in WT). In contrast to WT, P-LHCII is not able to interact with PSI in *nsi*
808 under state 2 conditions. The phenotype may result from defects in Lys acetylation of
809 (i) PSAH and LHCII, which may hinder the PSI-LHCII interaction, or (ii) PSBP and
810 LHCII, which may result in a strong interaction between PSII and L-LHCII, or (iii)
811 proteins involved in chloroplast ion homeostasis (PSBP, KEA1/KEA2), which may be
812 required for the dynamic reorganization of thylakoid protein complexes.

813

814

Parsed Citations

Allahverdiyeva, Y., Suorsa, M., Rossi, F., Pavesi, A., Kater, M.M., Antonacci, A., Tadini, L., Pribil, M., Schneider, A., Wanner, G., et al. (2013). Arabidopsis plants lacking PsbQ and PsbR subunits of the oxygen-evolving complex show altered PSII super-complex organization and short-term adaptive mechanisms. Plant J. 75, 671-684.
Pubmed: Author and Title
Google Scholar: Author Only Title Only Author and Title

Allen, J.F. (1992). Protein phosphorylation in regulation of photosynthesis. Biochim. Biophys. Acta 1098, 275-335.
Pubmed: Author and Title
Google Scholar: Author Only Title Only Author and Title

Bellafiore, S., Barneche, F., Peltier, G., and Rochaix, J.-D. (2005). State transitions and light adaptation require chloroplast thylakoid protein kinase STN7. Nature 433, 892-895.
Pubmed: Author and Title
Google Scholar: Author Only Title Only Author and Title

Benson, S.L., Maheswaran, P., Ware, M.A., Hunter, C.N., Horton, P., Jansson, S., Ruban, A.V., and Johnson, M.P. (2015). An intact light harvesting complex I antenna system is required for complete state transitions in Arabidopsis. Nature Plants, 15176.
Pubmed: Author and Title
Google Scholar: Author Only Title Only Author and Title

Bennett, J., Steinback, K.E., and Arntzen, C.J. (1980) Chloroplast phosphoproteins: regulation of excitation energy transfer by phosphorylation of thylakoid membrane polypeptides. Proc. Natl. Acad. Sci. USA. 77, 5253-7.
Pubmed: Author and Title
Google Scholar: Author Only Title Only Author and Title

Boersema, P.J., Raijmakers, R., Lemeer, S., Mohammed, S., and Heck, A.J.R. (2009). Multiplex peptide stable isotope dimethyl labeling for quantitative proteomics. Nat. Protoc. 4, 484-494.
Pubmed: Author and Title
Google Scholar: Author Only Title Only Author and Title

Bonaventura, C., and Myers, J. (1969). Fluorescence and oxygen evolution from Chlorella pyrenoidosa. Biochim. Biophys. Acta 189, 366-383.
Pubmed: Author and Title
Google Scholar: Author Only Title Only Author and Title

Brandizzi, F., Frangne, N., Marc-Martin, S., Hawes, C., Neuhaus, J.-M., and Paris, N. (2002). The destination for single-pass membrane proteins is influenced markedly by the length of the hydrophobic domain. Plant Cell 14, 1077-1092.
Pubmed: Author and Title
Google Scholar: Author Only Title Only Author and Title

Cardol, P., Gloire, G., Havaux, M., Remacle, C., Matagne, R., and Franck, F. (2003). Photosynthesis and state transitions in mitochondrial mutants of Chlamydomonas reinhardtii affected in respiration. Plant Physiol. 133, 2010-20.
Pubmed: Author and Title
Google Scholar: Author Only Title Only Author and Title

Chuartzman, S.G., Nevo ,R., Shimoni, E., Charuvi, D., Kiss, V., Ohad, I., Brumfeld, V., and Reich, Z. (2008). Thylakoid membrane remodeling during state transitions in Arabidopsis. Plant Cell 20, 1029-39.
Pubmed: Author and Title
Google Scholar: Author Only Title Only Author and Title

Cox, J., and Mann, M. (2008). MaxQuant enables high peptide identification rates, individualized p.p.b.-range mass accuracies and proteome-wide protein quantification. Nat. Biotechnol. 26, 1367-1372.
Pubmed: Author and Title
Google Scholar: Author Only Title Only Author and Title

Crepin, A., and Caffarri, S. (2015). The specific localizations of phosphorylated Lhcb1 and Lhcb2 isoforms reveal the role of Lhcb2 in the formation of the PSI-LHCII supercomplex in Arabidopsis during state transitions. Biochim. Biophys. Acta 1847, 1539-1548.
Pubmed: Author and Title
Google Scholar: Author Only Title Only Author and Title

Demmig-Adams, B. (1990). Carotenoids and photoprotection in plants: A role for the xanthophyll zeaxanthin. Biochim. Biophys. Acta 1020, 1-24.
Pubmed: Author and Title
Google Scholar: Author Only Title Only Author and Title

Depège, N., Bellafiore, S., and Rochaix, J.-D. (2003). Role of chloroplast protein kinase Stt7 in LHCII phosphorylation and state transition in Chlamydomonas. Science 299, 1572-1575.
Pubmed: Author and Title
Google Scholar: Author Only Title Only Author and Title

Dinh, T.V., Bienvenut, W.V., Linster, E., Feldman-Salit, A., Jung, V.A., Meinnel, T., Hell, R., Giglione, C., and Wirtz, M. (2015). Molecular identification and functional characterization of the first Nα-acetyltransferase in plastids by global acetylome profiling. Proteomics 15,

2426-2435.
Pubmed: Author and Title
Google Scholar: Author Only Title Only Author and Title

Finkemeier, I., Laxa, M., Miguet, L., Howden, A.J.M., and Sweetlove, L.J. (2011). Proteins of diverse function and subcellular location are lysine acetylated in Arabidopsis. Plant Physiol. 155, 1779-1790.
Pubmed: Author and Title
Google Scholar: Author Only Title Only Author and Title

Fristedt, R., Herdean, A., Blaby-Haas, C.E., Mamedov, F., Merchant, S.S., Last, R.L., and Lundin, B. (2015). PHOTOSYSTEM II PROTEIN33, a protein conserved in the plastid lineage, is associated with the chloroplast thylakoid membrane and provides stability to photosystem II supercomplexes in Arabidopsis. Plant Physiol. 167, 481-92. Erratum in: Plant Physiol. 2017 173, 2411.
Pubmed: Author and Title
Google Scholar: Author Only Title Only Author and Title

Fristedt, R., Trotta, A., Suorsa, M., Nilsson, A.K., Croce, R., Aro, E.M., and Lundin B. (2017). PSB33 sustains photosystem II D1 protein under fluctuating light conditions. J. Exp. Bot. 68, 4281-4293.
Pubmed: Author and Title
Google Scholar: Author Only Title Only Author and Title

Galka, P., Santabarbara, S., Khuong, T.T.H., Degand, H., Morsomme, P., Jennings, R.C., Boekema, E.J., and Caffarri, S. (2012). Functional analyses of the plant photosystem I-light-harvesting complex II supercomplex reveal that light-harvesting complex II loosely bound to photosystem II is a very efficient antenna for photosystem I in state II. Plant Cell 24, 2963-2978.
Pubmed: Author and Title
Google Scholar: Author Only Title Only Author and Title

Gawroński, P., Górecka, M., Bederska, M., Rusaczonek, A., Ślesak, I., Kruk, J., and Karpiński, S. (2013). Isochorismate synthase 1 is required for thylakoid organization, optimal plastoquinone redox status, and state transitions in Arabidopsis thaliana. J. Exp. Bot. 64, 3669-3679.
Pubmed: Author and Title
Google Scholar: Author Only Title Only Author and Title

Genty, B., Briantais, J., and Baker, N.R. (1989). The relationship between the quantum yield of photosynthetic electron transport and quenching of chlorophyll fluorescence. Biochim. Biophys. Acta 990, 87-92.
Pubmed: Author and Title
Google Scholar: Author Only Title Only Author and Title

Grieco, M., Tikkanen, M., Paakkarinen, V., Kangasjärvi, S., and Aro, E.-M. (2012). Steady-state phosphorylation of light-harvesting complex II proteins preserves photosystem I under fluctuating white light. Plant Physiol. 160, 1896-1910.
Pubmed: Author and Title
Google Scholar: Author Only Title Only Author and Title

Hartl, M., Füßl, M., Boersema, P., Jost, J.O., Kramer, K., Bakirbas, A., Sindlinger, J., Plöchinger, M., Leister, D., Uhrig, G., et al. (2017). Lysine acetylome profiling uncovers novel histone deacetylase substrate proteins in Arabidopsis. Mol. Syst. Biol. 13, 949.
Pubmed: Author and Title
Google Scholar: Author Only Title Only Author and Title

Hartl, M., König, A.-C., and Finkemeier, I. (2015). Identification of lysine-acetylated mitochondrial proteins and their acetylation sites. In Plant Mitochondria: Methods and Protocols, Whelan, J., and Murcha, M. eds., (New York: Humana Press) pp. 107-121.
Pubmed: Author and Title
Google Scholar: Author Only Title Only Author and Title

Ifuku, K., Ishihara, S., Shimamoto, R., Ido, K., and Sato, F. (2008). Structure, function, and evolution of the PsbP protein family in higher plants. Photosynth. Res. 98, 427-437.
Pubmed: Author and Title
Google Scholar: Author Only Title Only Author and Title

Ifuku, K., Nakatsu, T., Shimamoto, R., Yamamoto, Y., Ishihara, S., Kato, H., and Sato, F. (2005). Structure and function of the PsbP protein of Photosystem II from higher plants. Photosynth. Res. 84, 251-255.
Pubmed: Author and Title
Google Scholar: Author Only Title Only Author and Title

Inskeep, W.P., and Bloom, P.R. (1985). Extinction coefficients of chlorophylls a and b in N,N-dimethylformamide and 80% acetone. Plant Physiol. 77, 483-485.
Pubmed: Author and Title
Google Scholar: Author Only Title Only Author and Title

Järvi, S., Suorsa, M., Paakkarinen, V., and Aro, E.-M. (2011). Optimized native gel systems for separation of thylakoid protein complexes: Novel super- and mega-complexes. Biochem. J. 439, 207-214.
Pubmed: Author and Title
Google Scholar: Author Only Title Only Author and Title

Kaňa, R., and Govindjee. (2016). Role of ions in the regulation of light-harvesting. Front. Plant Sci. 7, 1849.
Pubmed: Author and Title
Google Scholar: Author Only Title Only Author and Title

Kettunen, R., Tyystjärvi, E., and Aro, E.-M. (1996). Degradation pattern of photosystem II reaction center protein D1 in intact leaves: The major photoinhibition-induced cleavage site in D1 polypeptide is located amino terminally of the DE loop. Plant Physiol. 111, 1183-1190.
Pubmed: Author and Title
Google Scholar: Author Only Title Only Author and Title

Klughammer, C., and Schreiber, U. (1994). An improved method, using saturating light pulses, for the determination of photosystem I quantum yield via P700+-absorbance changes at 830 nm. Planta 192, 261-268.
Pubmed: Author and Title
Google Scholar: Author Only Title Only Author and Title

Kouřil, R., Zygadlo, A., Arteni, A.A., De Wit, C.D., Dekker, J.P., Jensen, P.E., Scheller, H.V., and Boekema, E.J. (2005). Structural characterization of a complex of photosystem I and light-harvesting complex II of Arabidopsis thaliana. Biochemistry 44, 10935-10940.
Pubmed: Author and Title
Google Scholar: Author Only Title Only Author and Title

Kramer, D.M., Johnson, G., Kiirats, O., and Edwards, G.E. (2004). New fluorescence parameters for the determination of QA redox state and excitation energy fluxes. Photosynth. Res. 79, 209-218.
Pubmed: Author and Title
Google Scholar: Author Only Title Only Author and Title

Kulak, N.A., Pichler, G., Paron, I., Nagaraj, N., and Mann, M. (2014). Minimal, encapsulated proteomic-sample processing applied to copy-number estimation in eukaryotic cells. Nat. Methods 11, 319-324.
Pubmed: Author and Title
Google Scholar: Author Only Title Only Author and Title

Kunz, H.H., Gierth, M., Herdean, A., Satoh-Cruz, M., Kramer, D.M., Spetea, C., and Schroeder, J.I. (2014) Plastidial transporters KEA1, -2, and -3 are essential for chloroplast osmoregulation, integrity, and pH regulation in Arabidopsis. Proc. Natl. Acad. Sci. USA 111, 7480-5.
Pubmed: Author and Title
Google Scholar: Author Only Title Only Author and Title

Laemmli, U.K. (1970). Cleavage of structural proteins during the assembly of the head of bacteriophage T4. Nature 227, 680-685.
Pubmed: Author and Title
Google Scholar: Author Only Title Only Author and Title

Lee, H.Y., Byeon, Y., Lee, K., Lee, H.-J., and Back, K. (2014). Cloning of Arabidopsis serotonin N-acetyltransferase and its role with caffeic acid O-methyltransferase in the biosynthesis of melatonin in vitro despite their different subcellular localizations. J. Pineal Res. 57, 418-426.
Pubmed: Author and Title
Google Scholar: Author Only Title Only Author and Title

Leoni, C., Pietrzykowska, M., Kiss, A.Z., Suorsa, M., Ceci, L.R., Aro, E.-M., and Jansson, S. (2013). Very rapid phosphorylation kinetics suggest a unique role for Lhcb2 during state transitions in Arabidopsis. Plant J. 76, 236-246.
Pubmed: Author and Title
Google Scholar: Author Only Title Only Author and Title

Longoni, P., Douchi, D., Cariti, F., Fucile, G., and Goldschmidt-Clermont, M. (2015). Phosphorylation of the light-harvesting complex II isoform Lhcb2 is central to state transitions. Plant Physiol. 169, 2874-2883.
Pubmed: Author and Title
Google Scholar: Author Only Title Only Author and Title

Lunde, C., Jensen, P.E., Haldrup, A., Knoetzel, J., and Scheller, H.V. (2000). The PSI-H subunit of photosystem I is essential for state transitions in plant photosynthesis. Nature 408, 613-615.
Pubmed: Author and Title
Google Scholar: Author Only Title Only Author and Title

McDonald, K.L. (2014). Out with the old and in with the new: Rapid specimen preparation procedures for electron microscopy of sectioned biological material. Protoplasma 251, 429-448.
Pubmed: Author and Title
Google Scholar: Author Only Title Only Author and Title

Moran, D.T., and Rowley, J.C. (1987). Biological specimen preparation for correlative light and electron microscopy. In Correlative microscopy in biology: instrumentation and methods, Hayat, M. A. ed., (New York: Academic Press) pp. 1-22.
Pubmed: Author and Title
Google Scholar: Author Only Title Only Author and Title

Morgan, M.J., Lehmann, M., Schwarzländer, M., Baxter, C.J., Sienkiewicz-Porzucek, A., Williams, T.C., Schauer, N., Fernie, A.R., Fricker, M.D., Ratcliffe, R.G., Sweetlove, L.J., and Finkemeier, I. (2008) Decrease in manganese superoxide dismutase leads to reduced root growth and affects tricarboxylic acid cycle flux and mitochondrial redox homeostasis. Plant Physiol. 147, 101-14.
Pubmed: Author and Title
Google Scholar: Author Only Title Only Author and Title

Murata, N. (1969). Control of excitation transfer in photosynthesis. I. Light-induced change of chlorophyll a fluoresence in Porphyridium cruentum. Biochim. Biophys. Acta 172, 242-251.
Pubmed: Author and Title
Google Scholar: Author Only Title Only Author and Title

Narusaka, M., Shiraishi, T., Iwabuchi, M., and Narusaka, Y. (2010). The floral inoculating protocol: A simplified Arabidopsis thaliana transformation method modified from floral dipping. Plant Biotechnol. 27, 349-351.
Pubmed: Author and Title
Google Scholar: Author Only Title Only Author and Title

Pesaresi, P., Hertle, A., Pribil, M., Kleine, T., Wagner, R., Strissel, H., Lhnatowicz, A., Bonardi, V., Scharfenberg, M., Schneider, A., Pfannschmidt, T., and Leister, D. (2009). Arabidopsis STN7 kinase provides a link between short- and long-term photosynthetic acclimation. Plant Cell 21, 2402-2423.
Pubmed: Author and Title
Google Scholar: Author Only Title Only Author and Title

Pietrzykowska, M., Suorsa, M., Semchonok, D.A., Tikkanen, M., Boekema, E.J., Aro, E.-M., and Jansson, S. (2014). The light-harvesting chlorophyll a/b binding proteins Lhcb1 and Lhcb2 play complementary roles during state transitions in Arabidopsis. Plant Cell 26, 3646-3660.
Pubmed: Author and Title
Google Scholar: Author Only Title Only Author and Title

Porra, R.J., Thompson, W.A., and Kriedemann, P.E. (1989). Determination of accurate extinction coefficients and simultaneous equations for assaying chlorophylls a and b extracted with four different solvents: verification of the concentration of chlorophyll standards by atomic absorption spectroscopy. Biochim. Biophys. Acta 975, 384-394.
Pubmed: Author and Title
Google Scholar: Author Only Title Only Author and Title

Pribil, M., Pesaresi, P., Hertle, A., Barbato, R., and Leister, D. (2010). Role of plastid protein phosphatase TAP38 in LHCII dephosphorylation and thylakoid electron flow. PloS Biol. 8.
Pubmed: Author and Title
Google Scholar: Author Only Title Only Author and Title

Rintamäki, E., Martinsuo, P., Pursiheimo, S., and Aro, E.M. (2000). Cooperative regulation of light-harvesting complex II phosphorylation via the plastoquinol and ferredoxin-thioredoxin system in chloroplasts. Proc. Natl. Acad. Sci. USA 97, 11644-11649.
Pubmed: Author and Title
Google Scholar: Author Only Title Only Author and Title

Ritchie, M.E., Phipson, B., Wu, D., Hu, Y., Law, C.W., Shi, W., and Smyth, G.K. (2015). Limma powers differential expression analyses for RNA-sequencing and microarray studies. Nucleic Acids Res. 43, e47.
Pubmed: Author and Title
Google Scholar: Author Only Title Only Author and Title

Rozhon, W., Mayerhofer, J., Petutschnig, E., Fujioka, S., and Jonak, C. (2010). ASKθ, a group-III Arabidopsis GSK3, functions in the brassinosteroid signalling pathway. Plant J. 62, 215-223.
Pubmed: Author and Title
Google Scholar: Author Only Title Only Author and Title

Ruban, A.V., and Johnson, M.P. (2009). Dynamics of higher plant photosystem cross-section associated with state transitions. Photosynth. Res. 99, 173-183.
Pubmed: Author and Title
Google Scholar: Author Only Title Only Author and Title

Sawaguchi, A., Ide, S., Goto, Y., Kawano, J.I., Oinuma, T., and Suganuma, T. (2001). A simple contrast enhancement by potassium permanganate oxidation for Lowicryl K4M ultrathin sections prepared by high pressure freezing/freeze substitution. J. Microsc. 201, 77-83.
Pubmed: Author and Title
Google Scholar: Author Only Title Only Author and Title

Schmidt, C., Beilsten-Edmands, V., Mohammed, S., and Robinson, C.V. (2017). Acetylation and phosphorylation control both local and global stability of the chloroplast F1 ATP synthase. Sci. Rep. 7.
Pubmed: Author and Title
Google Scholar: Author Only Title Only Author and Title

Schönfeld, C., Wobbe, L., Borgstädt, R., Kienast, A., Nixon, P.J., and Kruse, O. (2004). The nucleus-encoded protein MOC1 is essential for mitochondrial light acclimation in Chlamydomonas reinhardtii. J. Biol. Chem. 279, 50366-74.
Pubmed: Author and Title
Google Scholar: Author Only Title Only Author and Title

Schreiber U, Schliwa U and Bilger W (1986). Continuous recording of photochemical and non-photochemical chlorophyll fluorescence quenching with a new type of modulation fluorometer. Photosynth Res 10, 51–62.
Pubmed: Author and Title
Google Scholar: Author Only Title Only Author and Title

Seidel, J., Klockenbusch, C., and Schwarzer, D. (2016). Investigating deformylase and deacylase activity of mammalian and bacterial sirtuins. ChemBioChem 17, 398-402.
Pubmed: Author and Title
Google Scholar: Author Only Title Only Author and Title

Shapiguzov, A., Ingelsson, B., Samol, I., Andres, C., Kessler, F., Rochaix, J.-D., Vener, A.V., and Goldschmidt-Clermont, M. (2010). The PPH1 phosphatase is specifically involved in LHCII dephosphorylation and state transitions in Arabidopsis. Proc. Natl. Acad. Sci. USA 107, 4782-4787.
Pubmed: Author and Title
Google Scholar: Author Only Title Only Author and Title

Suorsa, M., Rantala, M., Mamedov, F., Lespinasse, M., Trotta, A., Grieco, M., Vuorio, E., Tikkanen, M., Järvi, S., and Aro, E.-M. (2015). Light acclimation involves dynamic re-organization of the pigment-protein megacomplexes in non-appressed thylakoid domains. Plant J. 84, 360-373.
Pubmed: Author and Title
Google Scholar: Author Only Title Only Author and Title

Tikkanen, M., Piippo, M., Suorsa, M., Sirpiö, S., Mulo, P., Vainonen, J., Vener, A.V., Allahverdiyeva, Y., and Aro, E.-M. (2006). State transitions revisited - A buffering system for dynamic low light acclimation of Arabidopsis. Plant Mol. Biol. 62, 795.
Pubmed: Author and Title
Google Scholar: Author Only Title Only Author and Title

Tyanova, S., Temu, T., and Cox, J. (2016a). The MaxQuant computational platform for mass spectrometry-based shotgun proteomics. Nat. Protoc. 11, 2301-2319.
Pubmed: Author and Title
Google Scholar: Author Only Title Only Author and Title

Tyanova, S., Temu, T., Sinitcyn, P., Carlson, A., Hein, M.Y., Geiger, T., Mann, M., and Cox, J. (2016b). The Perseus computational platform for comprehensive analysis of (prote)omics data. Nat. Methods 13, 731-740.
Pubmed: Author and Title
Google Scholar: Author Only Title Only Author and Title

Tyystjärvi, E., and Karunen, J. (1990). A microcomputer program and fast analog to digital converter card for the analysis of fluorescence induction transients. Photosynth. Res 26, 127-132.
Pubmed: Author and Title
Google Scholar: Author Only Title Only Author and Title

Wang, P., and Grimm, B. (2016). Comparative analysis of light-harvesting antennae and state transition in chlorina and cpSRP mutants. Plant Physiol. 172, 1519-1531.
Pubmed: Author and Title
Google Scholar: Author Only Title Only Author and Title

Vizcaíno, J.A., Csordas, A., Del-Toro, N., Dianes, J.A., Griss, J., Lavidas, I., Mayer, G., Perez-Riverol, Y., Reisinger, F., Ternent, T., et al. (2016). 2016 update of the PRIDE database and its related tools. Nucleic Acids Res. 44, D447-D456.
Pubmed: Author and Title
Google Scholar: Author Only Title Only Author and Title

Wiśniewski, J.R., Zougman, A., and Mann, M. (2009a). Combination of FASP and StageTip-based fractionation allows in-depth analysis of the hippocampal membrane proteome. J. Proteome Res. 8, 5674-5678.
Pubmed: Author and Title
Google Scholar: Author Only Title Only Author and Title

Wiśniewski, J.R., Zougman, A., Nagaraj, N., and Mann, M. (2009b). Universal sample preparation method for proteome analysis. Nat. Methods 6, 359-362.
Pubmed: Author and Title
Google Scholar: Author Only Title Only Author and Title

Wollman, F.A. (2001). State transitions reveal the dynamics and flexibility of the photosynthetic apparatus. EMBO J. 20, 3623-30.
Pubmed: Author and Title
Google Scholar: Author Only Title Only Author and Title

Wu, X., Oh, M., Schwarz, E.M., Larue, C.T., Sivaguru, M., Imai, B.S., Yau, P.M., Ort, D.R., and Huber, S.C. (2011). Lysine acetylation is a widespread protein modification for diverse proteins in Arabidopsis. Plant Physiol. 155, 1769-1778.
Pubmed: Author and Title
Google Scholar: Author Only Title Only Author and Title

Yi, X., Hargett, S.R., Frankel, L.K., and Bricker, T.M. (2009). The PsbP protein, but not the PsbQ protein, is required for normal thylakoid architecture in Arabidopsis thaliana. FEBS Lett. 583, 2142-2147.
Pubmed: Author and Title
Google Scholar: Author Only Title Only Author and Title

Zhang, S., and Scheller, H.V. (2004) Light-harvesting complex II binds to several small subunits of photosystem I. J. Biol. Chem. 279, 3180-7.
Pubmed: Author and Title
Google Scholar: Author Only Title Only Author and Title

Chloroplast acetyltransferase NSI is required for state transitions in Arabidopsis thaliana

Minna M. Koskela, Annika Brünje, Aiste Ivanauskaite, Magda Grabsztunowicz, Ines Lassowskat, Ulla Neumann, Trinh V. Dinh, Julia Sindlinger, Dirk Schwarzer, Markus Wirtz, Esa Tyystjarvi, Iris Finkemeier and Paula Mulo

Plant Cell; originally published online July 2, 2018;
DOI 10.1105/tpc.18.00155

This information is current as of August 6, 2018

Supplemental Data	**/content/suppl/2018/07/02/tpc.18.00155.DC1.html**
Permissions	https://www.copyright.com/ccc/openurl.do?sid=pd_hw1532298X&issn=1532298X&WT.mc_id=pd_hw1532298X
eTOCs	Sign up for eTOCs at: http://www.plantcell.org/cgi/alerts/ctmain
CiteTrack Alerts	Sign up for CiteTrack Alerts at: http://www.plantcell.org/cgi/alerts/ctmain
Subscription Information	Subscription Information for *The Plant Cell* and *Plant Physiology* is available at: http://www.aspb.org/publications/subscriptions.cfm

© American Society of Plant Biologists
ADVANCING THE SCIENCE OF PLANT BIOLOGY